PHYSICAL REVIEW E **85**, 021801 (2012)

Nonlinear effective-medium theory of disordered spring networks

M. Sheinman,[1,2] C. P. Broedersz,[1,2,3] and F. C. MacKintosh[1,2]
[1]*Department of Physics and Astronomy, Vrije Universiteit, Amsterdam, The Netherlands*
[2]*Kavli Institute for Theoretical Physics, University of California, Santa Barbara, California 93106, USA*
[3]*Lewis-Sigler Institute for Integrative Genomics and the Department of Physics, Princeton University, Princeton, New Jersey 08544, USA*
(Received 23 August 2011; published 8 February 2012)

Disordered soft materials, such as fibrous networks in biological contexts, exhibit a nonlinear elastic response. We study such nonlinear behavior with a minimal model for networks on lattice geometries with simple Hookian elements with disordered spring constant. By developing a mean-field approach to calculate the differential elastic bulk modulus for the macroscopic network response of such networks under large isotropic deformations, we provide insight into the origins of the strain stiffening and softening behavior of these systems. We find that the nonlinear mechanics depends only weakly on the lattice geometry and is governed by the average network connectivity. In particular, the nonlinear response is controlled by the isostatic connectivity, which depends strongly on the applied strain. Our predictions for the strain dependence of the isostatic point as well as the strain-dependent differential bulk modulus agree well with numerical results in both two and three dimensions. In addition, by using a mapping between the disordered network and a regular network with random forces, we calculate the nonaffine fluctuations of the deformation field and compare them to the numerical results. Finally, we discuss the limitations and implications of the developed theory.

DOI: 10.1103/PhysRevE.85.021801 PACS number(s): 87.10.Pq

I. INTRODUCTION

Rich elastic behavior is a common feature of many soft materials such as foams, granular packings, and soft glasses [1,2], as well as networks of protein fibers that form major structural components of cells and tissue [3–5]. One characteristic these varied systems share is their particular sensitivity to external stress; in densely jammed systems, for instance, the external pressure can cause the system to transition between rigid and floppy states [1,2,6–9], while reconstituted biological filamentous networks exhibit dramatic strain stiffening under shear [10–13]. This remarkable nonlinear elastic behavior of fiber networks has attracted much attention in the last decade; in addition to the physiological relevance of this nonlinear elastic response for cells and many biological tissues [14,15], these systems are also interesting from a fundamental perspective, owing to their unusual nonlinear materials properties [11–13,16–24], including negative normal stresses [25]. Understanding how their intrinsic disordered nature affects the elastic deformations is required for a complete theoretical description of their nonlinear mechanical behavior. Although structural disorder and inhomogeneous deformations clearly play a central role in jamming systems [2,7,26], their precise role in the nonlinear behavior of fibrous networks remains unclear [7,16,19,20,24,27,28].

Prior work on the nonlinear elasticity of random spring networks has focused on triangular lattices with internal stresses [29]. In the limit of small disorder, a perturbation theory was applied to describe the nonlinear elastic response of such systems with *small* dilution. It was shown numerically that the transition value of the mean coordination number, at which the network acquires rigidity, shifts with applied strain. Interestingly, the perturbation theory also appeared to capture the behavior observed numerically even for highly diluted networks since the bulk modulus was found to increase linearly with the mean coordination number beyond the rigidity percolation point. Recently, similar nonlinear behavior was analyzed for random spring networks in jammed configurations. Consistent with prior work on triangular lattices [29], it was shown that this nonlinear response is controlled by the central-force isostatic point [7]; this isostatic point characterizes the average connectivity z at which the number of central-force constraints balances the number of degrees of freedom in the system and is given by $z_0 = 2d$ in d dimensions [30]. For jammed systems, it was shown that the nonlinear response close to this isostatic point is well described by a mean-field scaling approach [7]. By contrast, the systems we consider here are not in jammed configurations, but instead fall in the class of lattice-based rigidity percolation problems [31–33]. For instance, the linear elastic response of fiber networks is also governed by the central-force isostatic point for a broad range of network connectivities, even with fibers with noncentral fiber bending interactions, but with non-mean-field behavior [34]. Motivated by these results, we investigate the nonlinear behavior of fiber networks in the limit of vanishing bending rigidity under large deformations.

Here, we investigate the nonlinear elastic response of random spring networks under isotropic expansion or compression over a broad range of network connectivities, both above and below the small strain isostatic point z_0, as illustrated in Fig. 1. From simulations we find that disordered *subisostatic* spring networks exhibit significant strain stiffening. We gain insight into the origins of this behavior by developing an effective-medium theory (EM theory) for the nonlinear responses of random spring networks on lattice geometries. The nonlinear behavior of these systems depends only weakly on network geometry and appears to be controlled largely by the mean network connectivity z and the applied strain ϵ. Within the framework of this central-force network model, the network's stiffness exhibits a transition on the two-dimensional phase diagram in ϵ and z, which characterizes the strain dependence of the isostatic point, as shown in Fig. 2. The

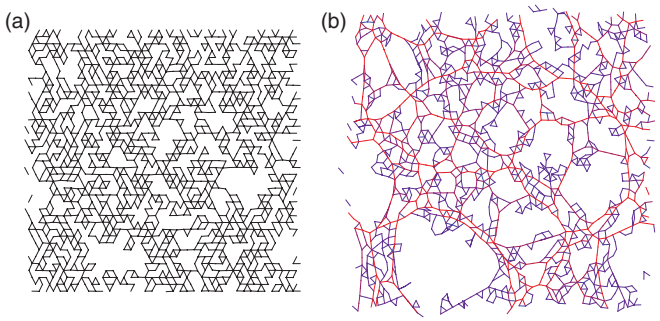

FIG. 1. (Color online) A small section of the relaxed (a) and expanded (b) diluted triangular lattice. The average coordination number in this example is $z = 3$. See [47] for a stiffening movie.

transition curve $z_c(\epsilon)$, representing the transition between a rigid and a floppy state, is derived using the EM theory and found to agree well with the numerical results. Interestingly, the mean-field solution predicts that a *superisostatic* central-force network loses rigidity and collapses beyond a threshold in compressional strain, as was observed for perfect two-dimensional triangular network in Monte Carlo simulations at low temperatures [35,36]. The theoretical predictions are verified using numerical calculation.

The mentioned above results for random spring networks may lend insight in the mechanics of biopolymer networks. The nonlinear elasticity of reconstituted networks of intracellular biopolymers such as filamentous actin (F-actin) and intermediate filaments has in many cases been accounted for by the affine entropic model [11,12,37,38]. In this model, network disorder is ignored by assuming a uniform (affine) deformation and, consequently, the nonlinear network response is directly determined by the nonlinear entropic force-extension behavior of the individual filaments. By contrast, there is increasing evidence that the strain-stiffening behavior of networks consisting of stiff thick fibers, such as collagen and bundled actin networks, is governed by collective nonaffine fiber bending deformations [13,28,39,40]. Despite extensive analytical and numerical investigations [7,16,19,20,24,27,41–46], the

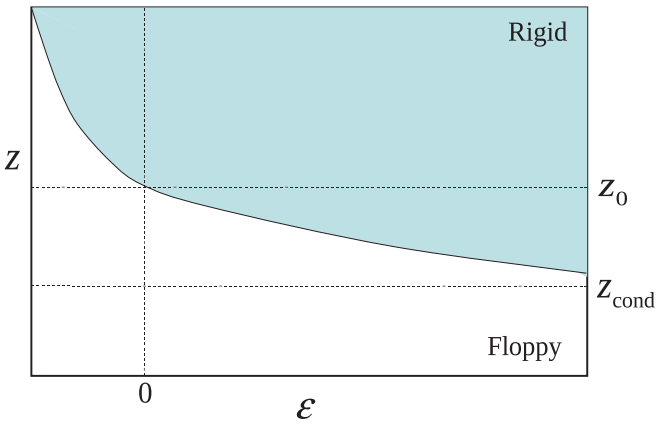

FIG. 2. (Color online) The schematic phase diagram for the rigidity of random spring networks under an isotropic strain ϵ. The central-force isostatic point z_0, the conductivity threshold z_{cond}, and the lower rigidity threshold in negative strain are indicated in the diagram.

principles of such network deformations and the resulting nonlinear network response are still unclear. To investigate the implications of our results on random spring networks for biological filamentous networks, we include a finite bending rigidity for the fibers in our network model. For sufficiently small bending rigidities, these networks exhibit nonlinear elastic behavior. However, in this case, the nonlinear behavior is not due to a transition between a floppy and a rigid state, but between a soft bending-dominated elastic behavior and a stiffer stretching-dominated behavior [16]. Both with and without bending rigidity, the nonlinear response is still governed by the central-force isostatic point.

The outline of the paper is as follows. In Sec. II, we define the model and summarize the applied approach and the main results of the paper. In Sec. III, we present the mean-field approach in detail, derive the differential bulk modulus of a system, analyze the nonaffine fluctuations, and, by using a self-consistency check, we identify the range of applicability of the performed approximations. In Sec. IV, we demonstrate the presented general method using a particular example of the diluted regular networks and compare the analytical predictions to the numerical results. We discuss the results and their implications and summarize in Sec. VI.

II. THE MODEL

In this paper, we analyze the nonlinear elastic behavior of a random central-force network on lattice geometries with varying connectivity. We start out with a model in which the bending energy of the fibers or bonds is ignored. This model will allow us to study the effects of finite strain on the central-force isostatic point z_c and the stretching energies of the bonds. To further simplify our model, we only consider isotropic expansional and compressional strains (see Fig. 1). The calculation of the elastic properties under nonlinear shear is complicated by the broken symmetry and is described elsewhere [48]. The network is constructed on an ordered lattice geometry in $d \geqslant 1$ dimensions. We capture the effects of disorder by a distribution of the spring constants associated to the bonds in the network. In this model, the rest lengths of all springs are chosen to be identical and equal to the lattice spacing ℓ_0.

Measuring all lengths in units of ℓ_0, the Hamiltonian of the system is given by

$$H = \frac{1}{2}\sum_{\langle ij\rangle}\mu_{ij}(|\mathbf{R}_i - \mathbf{R}_j| - 1)^2, \tag{1}$$

where $\mathbf{R}_i$ is the position of vertex i, $\langle ij\rangle$ denotes the summation over neighboring lattice vertices, and μ_{ij} is the stretching modulus for the bond between vertices i and j. The stretching moduli μ_{ij} are drawn independently from a known probability density $P(\mu_{ij})$.

A. Quantities of interest

Here, we investigate the elastic response of the network to an applied global expansion and compression strain

$$\epsilon = \frac{L' - L}{L}, \tag{2}$$

where L' and L are the linear size of the strained and unstrained networks, respectively. To quantify the nonlinear elastic response to the global bulk strain, we define the *nonlinear differential bulk modulus* as

$$B(\epsilon) \equiv \frac{n}{d^2}\frac{\partial^2 E(\epsilon)}{\partial \epsilon^2}, \tag{3}$$

where $E(\epsilon)$ is the average elastic energy per bond, n is the density of bonds in the unstrained and undiluted lattice, and d is dimension of the system. For example, for the face centered cubic (fcc) lattice $n = 2\sqrt{6}\ell_0^{-3}$, while for the triangular lattice $n = 2\sqrt{3}\ell_0^{-2}$.

This definition of the nonlinear bulk modulus has the following advantages:

(1) Other quantities, related to the nonlinear response of the system to a global strain, may be deduced from $B(\epsilon)$. For instance, the pressure

$$\Pi = -\frac{\partial U}{\partial V}, \tag{4}$$

where $U = NE$ is the total elastic energy, N is the total number of springs in the undiluted network, $V = V_0(1+\epsilon)^d$ is the system's volume, and V_0 is the total volume of the unstrained network. This pressure can be obtained directly from the nonlinear differential bulk modulus using

$$\Pi = -\frac{d}{(1+\epsilon)^{d-1}}\int_0^\epsilon B(\epsilon)d\epsilon. \tag{5}$$

(2) In the linear regime $\epsilon \to 0$, the *nonlinear* bulk modulus converges to

$$B(\epsilon \to 0) = V\frac{\partial^2 U}{\partial V^2}. \tag{6}$$

(3) If the material is composed of Hookian bonds and its deformation is affine, $B(\epsilon)$ is constant and equal to n/d^2 times the average spring constant of the network. Thus, by plotting $\frac{d^2}{n}B(\epsilon)$, one can easily compare the actual elastic properties to the affine predictions.

B. Numerical results

To study the nonlinear elastic response of random spring networks, we choose a specific realization of the spring constant probability density for networks on lattice geometries (see Sec. IV for a detailed discussion). In particular, we investigate bond-diluted network of springs with a modulus μ with the following probability density:

$$P(\mu_{ij}) = \mathcal{P}\delta(\mu_{ij} - \mu) + (1-\mathcal{P})\delta(\mu_{ij}). \tag{7}$$

Thus, either a bond with a stretch modulus μ is present with a probability $\mathcal{P}$, or absent with a probability $1-\mathcal{P}$. By varying $\mathcal{P}$, we can tune the connectivity, i.e., the mean number of springs z, which are attached to a crosslink of the network. Here, we study nonlinear elasticity of such bond-diluted networks on a triangular lattice in $d = 2$ and fcc lattice in $d = 3$.

The mechanical response of these networks is sensitive to the applied strain. We quantify this network response with a differential bulk modulus $B(z,\epsilon)$ as shown in Fig. 3. The qualitative behavior of the nonlinear bulk modulus is similar to the behavior of the bulk moduli in the linear regime, but with an isostatic point that shifts continuously to lower coordination numbers, as demonstrated in Fig. 3. The nonlinear response of the diluted central-force networks can be characterized by a two-dimensional (z,ϵ) phase diagram of the differential bulk modulus, as shown schematically in Fig. 2. The transition curve $z_c(z)$ separates the floppy and the rigid regions. From this, it can be understood that a subisostatic diluted regular network with central-force interactions exhibits a strain-stiffening behavior, from a floppy to a rigid structure, as a function of applied strain.

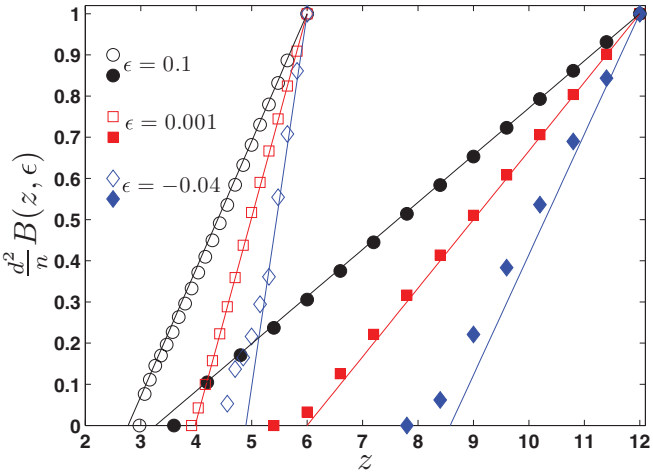

FIG. 3. (Color online) The nonlinear differential bulk modulus as a function of the coordination number for triangular (open symbols) and fcc (filled symbols) lattices for different strain values. The solid lines are the results of the EM theory [Eq. (49) or, in the explicit form, Eq. (B1)].

C. Mean-field approach

We gain insight in the nonlinear response of random spring networks [see Eq. (1)] by developing an effective medium approach for the high strain regime. This EM theory aims to provide a complete quantitative description of the nonlinear elastic response of a network under an external expansional and compressional strain ϵ. Our approach is a nonlinear extension of the EM approaches used to successfully describe the linear elastic response of diluted lattice-based networks [49], and goes beyond perturbative approaches for networks with small dilution [29]. The effective-medium theory for the linear elastic response of the disordered spring networks under small deformation was shown to predict the location of the critical coordination number and the elastic response far from it [49–51]. In other systems with non-central-force interactions, such as fiber bending models, the EM theory succeeded to capture the qualitative elastic behavior of the network [34].

The nonlinear EM approach developed here is based on a scheme to construct a mapping from the disordered system onto a perfect lattice system with uniform bond stiffness with the same network topology and strain ϵ, as illustrated in Fig. 4. This mapping is realized by an effective uniform central-force interaction $\mu_{ij} \to \widetilde{\mu}$. The effective parameter $\widetilde{\mu}$ is determined using a self-consistency requirement: replacing

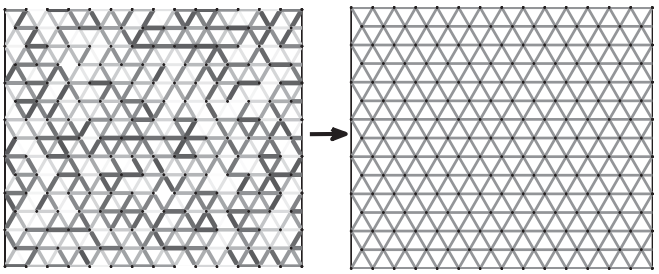

FIG. 4. Illustration of the EM approach. The network on the left represents the original system where the disorder in the spring constant is illustrated by the disorder of the width and the gray level of a bond. The right panel represents the EM with a regular, nondisordered structure.

a random bond in the uniform EM under strain with a bond drawn from the original probability density $P(\mu_{ij})$ results in a local fluctuation in the deformation field, which vanishes when averaged over the distribution $P(\mu_{ij})$. In addition, we assume that the fluctuations of the deformations are small compared to the distance between crosslinks. This approach leads to an integral equation, representing a disorder average Eq. (18) from which the effective parameter $\widetilde{\mu}(\epsilon)$ can be determined. Importantly, this effective parameter depends on strain, which gives rise to a nonlinear elastic response. By approximating the disordered elastic constants by this spatially homogeneous, yet strain-dependent effective parameter, we arrive at an energy expression for a homogeneously deforming network Eq. (12). The first and second derivatives of this expression with respect to ϵ give the pressure and the bulk modulus, respectively; from the latter, we obtain the transition between the floppy and rigid phases, i.e., the onset of nonlinearity.

III. EFFECTIVE-MEDIUM THEORY

We apply the EM theory method to a network subjected to a global expansion with a macroscopic isotropic strain ϵ. The position of a crosslink i is given by $\mathbf{R}_i = \mathbf{R}_i^0 + \mathbf{u}_i$, where $\mathbf{R}_i^0$ is the position in the unstrained configuration and $\mathbf{u}_i$ is the displacement due to the applied strain. The affine displacement is defined as $\mathbf{u}_i^{\text{aff}} - \mathbf{u}_j^{\text{aff}} = \epsilon \mathbf{r}_{ij}$, where $\mathbf{r}_{ij}$ is the vector from $\mathbf{R}_i^0$ to $\mathbf{R}_j^0$ in the undeformed reference state. Here, we allow for nonaffine displacements

$$\mathbf{v}_i \equiv \mathbf{u}_i - \mathbf{u}_i^{\text{aff}}, \tag{8}$$

given by the deviation of the displacement of network node i from its affine value. However, we assume that the resulting nonaffine relative displacements of neighboring nodes i and j are much smaller than the corresponding affine displacement:

$$|\mathbf{v}_{ij}| \equiv |\mathbf{v}_i - \mathbf{v}_j| \ll \left|\mathbf{u}_i^{\text{aff}} - \mathbf{u}_j^{\text{aff}}\right| = \ell_0 \epsilon. \tag{9}$$

Thus, we can expand the Hamiltonian around the affine strain configuration (small v_{ij}). Up to second order in v_{ij}, we arrive at [29,52]

$$H = \sum_{\langle ij \rangle} \mu_{ij} \left[\frac{1}{2}\epsilon^2 + \epsilon \mathbf{v}_{ij} \cdot \mathbf{r}_{ij} + \frac{1}{2} \frac{(\mathbf{v}_{ij} \cdot \mathbf{r}_{ij})^2 + \epsilon \mathbf{v}_{ij}^2}{1+\epsilon} \right]. \tag{10}$$

The first term represents the expansion and compression energy of the affine response, while the second and the third terms correspond to the energy difference due to the nonaffine deformation of the stretched and compressed bonds.

The expansion of the whole network corresponds to the global constraint

$$\sum_{\langle ij \rangle} \mathbf{v}_{ij} = 0. \tag{11}$$

Interestingly, the Hamiltonian for the network under a finite strain bears a resemblance with the Born model, which includes both isotropic and anisotropic pairwise interactions [53], as is the case here. However, as was noticed in [29], the model presented here is formally distinct from the Born model since here $\mathbf{v}_i$ is the displacement from the affinely deformed state and not from the undeformed configuration as is the case in the Born model. Thus, from our model Eq. (10) we see that a finite strain introduces additional interactions that penalize nonaffine deformations with a coupling parameter that is directly proportional to the strain ϵ.

To investigate the nonlinear elastic behavior of the model in Eq. (10), we set up an effective-medium theory. In the EM approach, we mimic the disordered system by the regular one with an effective parameter, i.e., $\mu_{ij} \to \widetilde{\mu}$. To deform the EM network similarly to the original system with the same global strain ϵ, one can use a Lagrange multiplier to ensure that the global constraint (11) is satisfied. In other words, the EM network may be globally expanded by applying the force that assures mechanical equilibrium for the affine $\mathbf{v}_{ij} = 0$ configuration. Thus, the EM system has the Hamiltonian, given by

$$H_{\text{EM}} = \sum_{\langle ij \rangle} \widetilde{\mu}(\epsilon) \left[\frac{1}{2}\epsilon^2 + \epsilon \mathbf{v}_{ij} \cdot \mathbf{r}_{ij} + \frac{1}{2} \frac{(\mathbf{v}_{ij} \cdot \mathbf{r}_{ij})^2 + \epsilon \mathbf{v}_{ij}^2}{1+\epsilon} \right] + \boldsymbol{\Lambda}_{ij} \cdot \mathbf{v}_{ij}, \tag{12}$$

where $\boldsymbol{\Lambda}_{ij} = -\widetilde{\mu}\epsilon \mathbf{r}_{ij}$. To calculate the effective parameter $\widetilde{\mu}$, we demand self-consistency of the EM [49]. The self-consistency requirement in this context can be formulated as follows: the nonaffine displacement induced by the replacement of a single bond in the EM vanishes on average,

$$\langle \mathbf{v}_{nm} \rangle = 0. \tag{13}$$

Here, the average is taken over the distribution of the nm bond in the original disordered system, i.e., according to the probability density $P(\mu_{nm})$. To calculate the displacement $\mathbf{v}_{nm}$ after the replacement, we solve the perturbed EM Hamiltonian that is given by

$$H_{\text{EM}} + \frac{1}{2}(\mu_{nm} - \widetilde{\mu}) \frac{(\mathbf{v}_{nm} \cdot \mathbf{r}_{nm})^2 + \epsilon \mathbf{v}_{nm}^2}{1+\epsilon} + \mathbf{v}_{nm} \cdot \mathbf{r}_{nm} \epsilon (\mu_{nm} - \widetilde{\mu}). \tag{14}$$

In the configuration that minimizes the energy, the displacement of the nm bond is given by

$$\mathbf{v}_{nm} = \frac{\mathbf{r}_{nm} \epsilon (\mu_{nm} - \widetilde{\mu})}{\mu_{\text{EM}} + \mu_{nm} - \widetilde{\mu}}, \tag{15}$$

where $\mu_{\rm EM}$ is the displacement of the nm bond in the *unperturbed* EM network due to a unit force acting along the nm bond. As detailed in Appendix A, it is given by

$$\mu_{\rm EM} = \frac{\widetilde{\mu}(\epsilon)}{a(\epsilon)}, \tag{16}$$

where $a(\epsilon)$ is given in Eq. (A6) and may be approximated for a highly coordinated lattice by

$$a(\epsilon) \approx \frac{2d(1+\epsilon)}{\mathcal{Z}}\left[1-\frac{\epsilon}{d}\left(\frac{1}{\frac{3}{2+d}+\epsilon}+\frac{d-1}{\frac{1}{2+d}+\epsilon}\right)\right]. \tag{17}$$

Given Eqs. (15) and (16), the self-consistency Eq. (13) leads to the following equation for the effective parameter:[1]

$$\int_0^\infty \frac{1-\widetilde{\mu}(\epsilon)/\mu_{ij}}{\frac{1}{a(\epsilon)}+1-\widetilde{\mu}(\epsilon)/\mu_{ij}} P(\mu_{ij})d\mu_{ij} = 0. \tag{18}$$

Importantly, in contrast to the linear EM, here the effective parameter $\widetilde{\mu}(\epsilon)$ can not be interpreted as the effective spring constant of the bonds in the EM. However, using the expression for $\widetilde{\mu}(\epsilon)$, one can determine the elastic properties of the original disordered system as follows. Since the equilibrium configuration of the regular EM network is given by the affine expansion $\mathbf{v}_{ij} = 0$, its energy (per bond) is given by

$$E_{\rm EM}(\epsilon) = H_{\rm EM}(\mathbf{v}_{ij}=0) = \tfrac{1}{2}\widetilde{\mu}(\epsilon)\epsilon^2. \tag{19}$$

The last expression may be interpreted as an approximation for the original system's energy up to correction terms. These terms appear since the energy is defined as

$$E_{\rm EM}(\epsilon) = \frac{d^2}{n}\int_0^\epsilon\int_0^{\epsilon'} B_{\rm EM}(\epsilon'')d\epsilon''\epsilon' \tag{20}$$

or

$$E_{\rm EM}(\epsilon) = \frac{(1+\epsilon)^d}{n}\int_0^\epsilon \Pi_{\rm EM}(\epsilon')\epsilon'. \tag{21}$$

Thus, for $z < z_0$, it includes the integration in the floppy phase, where the EM theory breaks down and predicts nonphysical elastic properties. To calculate the correction terms, we calculate first the floppy and rigid phases separation curve and then subtract from the expression (19) the integration in the floppy phase. This procedure depends on the assumption about the order of the phase transition. The nonlinear EMT presented here can not predict the order of the transition. Although the numerical results seem to agree better with a second order transition assumption, we can not completely rule out a first order transition. The assumed transition order affects the transition curves in the EM theory, but does not affect the predicted values of the bulk modulus above the transition. In what follows, we show the results of two assumptions about the order of the transition.

For a given mean coordination number and the transition order assumption, the transition strain value $\epsilon_c(z)$ may be found as follows. If the transition is first order, one requires that the energy and its first derivative vanish at the transition point. By contrast, if the transition is second order, one requires that the energy and its first and second derivatives vanish at the transition point. These two possible assumptions about the transition order result in different transition curves (z_c,ϵ_c). We define them as (z_{c_1},ϵ_{c_1}) for the first order transition case and (z_{c_2},ϵ_{c_2}) for the second order transition case. Since the order of the transition can not be deduced from the EM theory, described here, we will analyze both options. In Sec. IV, we calculate both transition curves for the particular example of the diluted regular networks and compare them to the numerical results.

The nonlinear bulk modulus, defined in Eq. (3), does not depend on the transition order and may be approximated by the EM approach using Eqs. (19) and (20). It is given by

$$B_{\rm EM}(\epsilon) = \frac{n}{d^2}\frac{\partial^2}{\partial\epsilon^2}\left[\widetilde{\mu}(\epsilon)\frac{\epsilon^2}{2}\right], \tag{22}$$

where $\widetilde{\mu}(\epsilon)$ is given in Eq. (A6) and is approximated in Eq. (17). In the limit of small strain, given by $\epsilon \to 0$, the mean-field rigidity threshold of the network, $z_c(\epsilon\to 0) = 2d$, also does not depend on the transition order. This corresponds to the mean-field isostatic point [30,49]. In the limit of large strain $\epsilon \to \infty$, the mean-field rigidity threshold of the network does not depend on the transition order and is $z_c(\epsilon\to\infty) = 2$.

The proper energy and the pressure in the system can be obtained from $B_{\rm EM}(\epsilon)$ by integration from ϵ_c:

$$E_{\rm EM}(\epsilon) = \frac{d^2}{n}\int_{\epsilon_c}^{\epsilon}\int_{\epsilon_c}^{\epsilon'} B_{\rm EM}(\epsilon'')d\epsilon''d\epsilon' \tag{23}$$

and

$$\Pi_{\rm EM}(\epsilon) = \frac{d^2}{(1+\epsilon)^d}\int_{\epsilon_c}^{\epsilon} B_{\rm EM}(\epsilon')d\epsilon', \tag{24}$$

where ϵ_c is defined as ϵ_{c_1} or ϵ_{c_2} for the first and second order transition assumptions, respectively.

The approach presented in this section allows one to calculate the elastic parameters of a system with a given topology and elastic constant distribution in the nonlinear elastic regime. The nonlinear differential bulk modulus is given by Eq. (22), while Eq. (18) determines the effective parameter $\widetilde{\mu}(\epsilon)$. Equation (18) may be solved numerically for any realization of the spring constant probability density $P(\mu_{ij})$. In Sec. IV, we demonstrate the presented method using the particular example of diluted regular networks when Eq. (18) can be easily solved analytically.

A. Mapping fluctuations to random forces

Within the EM approach, described above, a deviation of the spring constant of a given bond from the EM spring constant is described as an additional force dipole that acts on this bond. Therefore, the disorder of the spring constant may be mapped to the disorder of the force dipoles, which act on the regular EM in the EM theory approximation. More specifically, the replacement of the EM spring between nodes i and j by the spring with the elastic constant μ_{ij} is equivalent to the force

$$\mathbf{f}_n^{ij} = \epsilon\frac{\widetilde{\mu}-\mu_{ij}}{\frac{\widetilde{\mu}}{a(\epsilon)}-\widetilde{\mu}+\mu_{ij}}\frac{\widetilde{\mu}}{a(\epsilon)}(\delta_{i,n}-\delta_{j,n})\mathbf{r}_{ij} \tag{25}$$

[1] In the linear regime, Eq. (18) reduces to Eq. (9) in Ref. [49].

acting along the bond. Due to the self-consistence requirement (13), the average force is zero,

$$\left\langle \mathbf{f}_n^{ij} \right\rangle = 0 \tag{26}$$

and, since we assumed that there is no correlation between spring constants on distinct bonds, the associated forces are also uncorrelated:

$$\left\langle \mathbf{f}_n^{ij} \cdot \mathbf{f}_n^{i'j'} \right\rangle = \delta_{i,i'}\delta_{j,j'}\left\langle \left(\mathbf{f}_n^{ij}\right)^2 \right\rangle. \tag{27}$$

The obtained regular lattice (EM) with random forces is equivalent to *model B* in Ref. [54] (in contrast to the original system, which is defined as *model A* in Ref. [54]) and may thus be treated similarly. In particular, the nonaffinity correlation function of the strain field may be evaluated within this model. The described mapping has the same level of approximation as the EM approximation. However, this mapping completes the EM theory in the sense that it allows us to calculate all the correlation functions. In the following, we provide two examples of the usefulness of this mapping by calculating two important one-point correlation functions: the average nonaffine displacements and their nonlinear, differential analog.

B. Correlation functions

It is known that the rigidity percolation transition in the small-strain limit is accompanied by highly nonaffine network deformations [7,33,34]. As we show in this work, the nonaffine deformation field is responsible for the strain-stiffening behavior of the disordered spring networks. The mapping, described in Sec. III A, allows us to calculate any correlation function of the displacement field.

1. Nonaffinity parameter

Several methods have been proposed to quantify the deviation from a uniform (affine) strain field [16,42,54,55]. A useful parameter for the nonaffinity characterization is the average deviation from the affine configuration

$$\Gamma = \frac{1}{\epsilon^2}\langle \mathbf{v}_n^2 \rangle_n, \tag{28}$$

where $\langle \ldots \rangle_n$ denotes the average over all vertices. In the following, we calculate Γ using the EM approach including the mapping described in Sec. III A.

The Fourier transform of the force (25) is given by

$$\mathbf{f}^{ij}(\mathbf{k}) = \epsilon \frac{\widetilde{\mu} - \mu_{ij}}{\frac{\widetilde{\mu}}{a(\epsilon)} - \widetilde{\mu} + \mu_{ij}} \frac{\widetilde{\mu}}{a(\epsilon)} (e^{i\mathbf{k}\cdot\mathbf{R}_i} - e^{i\mathbf{k}\cdot\mathbf{R}_j})\mathbf{r}_{ij}. \tag{29}$$

Thus, the Fourier transform of the displacement field from the affine configuration due to this force is given by

$$\mathbf{v}(\mathbf{k}) = -\sum_{\langle ij \rangle} D^{-1}(\mathbf{k})\mathbf{f}^{ij}(\mathbf{k}) = \frac{\epsilon(1+\epsilon)}{a(\epsilon)} \times \sum_{\langle ij \rangle} \frac{\frac{\widetilde{\mu} - \mu_{ij}}{\frac{\widetilde{\mu}}{a(\epsilon)} - \widetilde{\mu} + \mu_{ij}} (e^{i\mathbf{k}\cdot\mathbf{R}_i} - e^{i\mathbf{k}\cdot\mathbf{R}_j})\mathbf{r}_{ij}}{\sum_{\mathbf{r}} (\mathbf{r} \otimes \mathbf{r} + \epsilon \mathbb{1})(1 - e^{i\mathbf{k}\cdot\mathbf{r}})}, \tag{30}$$

or in real space

$$\mathbf{v}_n = \frac{\epsilon(1+\epsilon)}{N a(\epsilon)} \sum_{\langle ij \rangle, \mathbf{k}} \frac{\frac{\widetilde{\mu} - \mu_{ij}}{\frac{\widetilde{\mu}}{a(\epsilon)} - \widetilde{\mu} + \mu_{ij}} (e^{i\mathbf{k}\cdot\mathbf{R}_i} - e^{i\mathbf{k}\cdot\mathbf{R}_j}) e^{-i\mathbf{k}\cdot\mathbf{R}_n} \mathbf{r}_{ij}}{\sum_{\mathbf{r}} (\mathbf{r} \otimes \mathbf{r} + \epsilon \mathbb{1})(1 - e^{i\mathbf{k}\cdot\mathbf{r}})}. \tag{31}$$

Since the forces are independent and identically distributed random variables, the variance of the displacement from the affine configuration of every network crosslink is given by

$$\langle \mathbf{v}_n^2 \rangle_n = \frac{1}{2}\left[\frac{\epsilon\,(1+\epsilon)}{a\,(\epsilon)}\right]^2 \left\langle \left(\frac{\widetilde{\mu} - \mu_{ij}}{\frac{\widetilde{\mu}}{a(\epsilon)} - \widetilde{\mu} + \mu_{ij}} \right)^2 \right\rangle \times \frac{1}{N} \sum_{\mathbf{r},\mathbf{k}} \left| \frac{1 - e^{i\mathbf{k}\cdot\mathbf{r}}}{\sum_{\mathbf{r}} (\mathbf{r} \otimes \mathbf{r} + \epsilon \mathbb{1})(1 - e^{i\mathbf{k}\cdot\mathbf{r}})} \mathbf{r} \right|^2. \tag{32}$$

The same approximation of highly coordinated lattice that was used to derive Eq. (A7) now gives

$$\langle \mathbf{v}_n^2 \rangle_n \simeq \frac{d\epsilon^2\,(1+\epsilon)^2}{2\mathcal{Z}a^2\,(\epsilon)} \left\langle \left(\frac{\widetilde{\mu} - \mu_{ij}}{\frac{\widetilde{\mu}}{a(\epsilon)} - \widetilde{\mu} + \mu_{ij}} \right)^2 \right\rangle \times \left[\frac{\frac{3}{2+d}}{\left(\frac{3}{2+d} + \epsilon\right)^2} + \frac{\frac{d-1}{2+d}}{\left(\frac{1}{2+d} + \epsilon\right)^2} \right] \frac{\sum_{\mathbf{k}} \frac{1}{k^2}}{N}. \tag{33}$$

The sum over $\mathbf{k}$ may be estimated for any dimension

$$\frac{1}{N}\sum_{\mathbf{k}} \frac{1}{k^2} = A_d \ell_0^2 f_d\,(N)\,, \tag{34}$$

where

$$f_d\,(N) = \begin{cases} \frac{d}{2-d} N^{\frac{2}{d}-1}, & d < 2 \\ \ln N, & d = 2 \\ \frac{d}{d-2}, & d > 2 \end{cases} \tag{35}$$

and

$$A_d = \frac{\frac{1}{N}\sum_{\mathbf{k}} \frac{1}{k^2}}{\frac{1}{\int_{1/L}^{1/\ell_0} k^{d-1} dk} \int_{1/L}^{1/\ell_0} \frac{k^{d-1}}{k^2} dk} = O\,(1) \tag{36}$$

is a dimensionless parameter, which depends weakly on the lattice geometry (for instance, $A_2 \simeq 0.36$ for the triangular lattice). As defined above, ℓ_0 is the rest length of a bond (throughout this paper, this quantity was set to unity, but is shown here explicitly to emphasize the cutoff of the integral in Fourier space and the units of the nonaffine parameter) and $L = \ell_0 N^{1/d}$ is the size of the unstrained network. In sum, the nonaffinity parameter is given by

$$\Gamma\,(\epsilon) \simeq A_d \ell_0^2 \frac{d\,(1+\epsilon)^2}{2\mathcal{Z}a^2\,(\epsilon)} \left\langle \left(\frac{\widetilde{\mu} - \mu_{ij}}{\frac{\widetilde{\mu}}{a(\epsilon)} - \widetilde{\mu} + \mu_{ij}} \right)^2 \right\rangle \times \left[\frac{\frac{3}{2+d}}{\left(\frac{3}{2+d} + \epsilon\right)^2} + \frac{\frac{d-1}{2+d}}{\left(\frac{1}{2+d} + \epsilon\right)^2} \right] f_d(N). \tag{37}$$

2. Differential nonaffinity parameter

In the nonlinear regime, the more interesting quantity is the differential nonaffinity fluctuation defined as

$$\delta\Gamma(\epsilon) = \left\langle \left[\lim_{\Delta\epsilon\to 0} \frac{\mathbf{v}_n(\epsilon+\Delta\epsilon) - \frac{1+\epsilon+\Delta\epsilon}{1+\epsilon}\mathbf{v}_n(\epsilon)}{\Delta\epsilon} \right]^2 \right\rangle_n = \left\langle \left(\frac{d\mathbf{v}_n(\epsilon)}{d\epsilon} - \frac{\mathbf{v}_n(\epsilon)}{1+\epsilon} \right)^2 \right\rangle_n = \left\langle \left(\frac{d\mathbf{v}_n(\epsilon)}{d\epsilon} \right)^2 \right\rangle_n - \frac{1}{1+\epsilon}\frac{d[\epsilon\Gamma(\epsilon)]}{d\epsilon} + \left(\frac{\epsilon}{1+\epsilon} \right)^2 \Gamma(\epsilon). \quad (38)$$

The first term in the last expression is calculated in Appendix C, while the last two may be easily deduced from Eq. (37).

C. Ginzburg criterion

Although the mean-field approach is not a controlled approximation and has no small parameter, one can check for self-consistency of the assumption of small fluctuations [56]. In our case, we assume small relative deviations of the EM from the affine strain field [see Eq. (10)]:

$$\frac{\langle \mathbf{v}_{nm}^2 \rangle_{\langle nm\rangle}}{\epsilon^2} \ll 1, \quad (39)$$

where $\langle \ldots \rangle_{\langle nm\rangle}$ is the average over all connected nodes of the EM network. Therefore, it is instructive to analyze the behavior of the two point, nearest neighbor (NN) correlation function. By using the same mapping to the random forces model as above, one gets

$$\Gamma_{\mathrm{NN}} = \frac{\langle \mathbf{v}_{nm}^2 \rangle_{\langle nm\rangle}}{\epsilon^2} = \frac{\Gamma}{A_d f_d}\frac{B_d}{d^2}, \quad (40)$$

where

$$B_d = \frac{1}{N}\sum_{\mathbf{k}} k^2 \simeq \frac{\int_{1/L}^{1/\ell_0} k^{d-1}k^2 dk}{\int_{1/L}^{1/\ell_0} k^{d-1}dk}. \quad (41)$$

The nonlinear, differential version of Γ_{NN}, defined as

$$\delta\Gamma_{\mathrm{NN}} = \left\langle \left[\lim_{\Delta\epsilon\to 0} \frac{\mathbf{v}_{nm}(\epsilon+\Delta\epsilon) - \frac{1+\epsilon+\Delta\epsilon}{1+\epsilon}\mathbf{v}_{nm}(\epsilon)}{\Delta\epsilon} \right]^2 \right\rangle_{\langle nm\rangle}, \quad (42)$$

is given by

$$\delta\Gamma_{\mathrm{NN}} = \frac{\delta\Gamma}{A_d f_d} B_d. \quad (43)$$

In Sec. IV D, we analyze the nonaffinity parameters for the particular example of the diluted regular networks and compare the analytical results with the numerical simulations.

IV. DILUTED REGULAR NETWORKS

A significant understanding of different physical phenomena in disordered systems, including percolation [57,58] and the elastic behavior of amorphous materials [58], was achieved by modeling the topological disorder by a random dilution of a regular structure. Motivated by this, we demonstrate the mean-field solution presented above using the particular example of bond-diluted regular networks. The probability density for the spring constants for such a network is given in Eq. (7). Networks of this kind are referred to as diluted spring networks or the central-force elastic percolation model. The linear elastic response of this model has been extensively studied [32,49]. Here, we show how these results generalize for large strain values. Before presenting the full mean-field solution for these networks, below we briefly sum up the known relevant results in the small strain regime and discuss the infinite strain limit expectations from the nonlinear EM theory.

A. Zero strain limit

The average coordination number for bond-diluted networks is defined as

$$z = \left\langle \sum_j (1 - \delta_{\mu_{ij},0}) \right\rangle_i = \mathcal{Z}\mathcal{P}, \quad (44)$$

where $\langle \ldots \rangle_i$ denotes an average over all network vertices and $\mathcal{Z}$ is the coordination number given that all existing springs have a nonzero spring constant. In the following, the so-called isostatic threshold of the average coordination number $z_0 \equiv z_c(\epsilon \to 0)$, the network is floppy [30,52].

For the unstressed reference state and zero strain limit, Maxwell introduced a mean-field counting argument for this threshold coordination number at which the number of degrees of freedom and the number of constraints due to the central-force interactions are equal. This yields an EM approximation for the isostatic coordination number

$$z_0 = 2d. \quad (45)$$

It was conjectured (see Ref. [49]) that the bulk modulus of the diluted network in the zero strain limit can be expressed in term of z_0 as

$$B(\epsilon \to 0) = \mu \frac{n}{d^2}\frac{z - z_0}{\mathcal{Z} - z_0}. \quad (46)$$

Equations (45) and (46) were derived [49] using the EM theory and were shown to predict well the location of the isostatic point and the elasticity of a diluted network far from its isostatic point.

B. Infinite strain limit

Before we turn to the full problem with arbitrary strain values, it is instructive to discuss our expectations in the infinite strain limit. In this limit, the rigidity threshold (isostatic point) can be expected to approach the conductivity threshold, denoted here by z_{cond}. By analogy with the behavior at small strains Eq. (46), we anticipate (and derive this result below) that in the large strain limit, the nonlinear bulk modulus is equal to

$$B(\epsilon \to \infty) = \mu \frac{n}{d^2}\frac{z - z_c(\epsilon\to\infty)}{\mathcal{Z} - z_c(\epsilon\to\infty)} = \mu \frac{n}{d^2}\frac{z - z_{\mathrm{cond}}}{\mathcal{Z} - z_{\mathrm{cond}}}. \quad (47)$$

The mean-field calculation [59] of the conductivity percolation and our calculation below in the infinite strain limit both suggest $z_c(\epsilon \to \infty) = 2$. We expect a deviation of the EM theory from the numerical calculation in the infinite strain

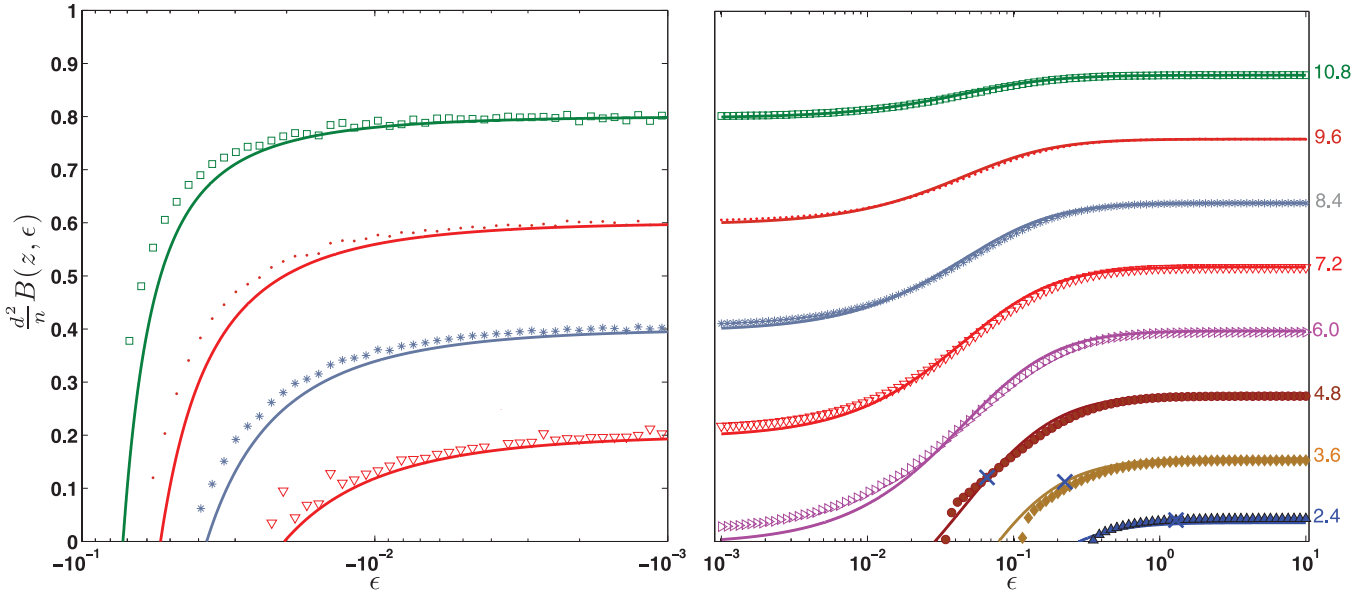

FIG. 5. (Color online) The nonlinear bulk modulus for the diluted fcc lattice as a function of the applied strain for different values of the average coordination number shown as labels next to the curves. The numerical data are depicted as symbols and the nonlinear EM theory predictions are shown as solid lines. Big crosses represent the location of the first order transition as predicted by Eq. (B2).

limit close to the conductivity percolation point due to the failure of the mean-field approach to predict the precise value of the conductivity threshold.

C. Full solution

Using Eq. (7), the solution for the self-consistent equation (18) is given by

$$\widetilde{\mu}(\epsilon) = \mu \frac{z - a(\epsilon)\mathcal{Z}}{\mathcal{Z} - a(\epsilon)\mathcal{Z}}, \tag{48}$$

where $a(\epsilon)$ is given in Eq. (A6) and is approximated in Eq. (17). The nonlinear differential bulk modulus of the original system may be approximated by the EM approach using Eqs. (22) and (48) and is given by

$$B_{\mathrm{EM}}(z,\epsilon) = \begin{cases} \mu \frac{n}{d^2} \frac{\partial^2}{\partial \epsilon^2} \left[\frac{z - a(\epsilon)\mathcal{Z}}{\mathcal{Z} - a(\epsilon)\mathcal{Z}} \frac{\epsilon^2}{2} \right], & \epsilon \geqslant \epsilon_c \\ 0, & \epsilon < \epsilon_c \end{cases} \tag{49}$$

where ϵ_c is defined as ϵ_{c_1} or ϵ_{c_2} for the first and second order transition assumptions, respectively. In Appendix B, we present the explicit result for the nonlinear differential bulk modulus and the transition curves (for both assumptions for the transition order), based on Eq. (49).

A comparison between this analytic prediction and the numerical results is shown in Figs. 5, 6, and 7. Below the conductivity percolation threshold $z < z_{\mathrm{cond}}$, a network, does not resist deformation for any strain and $B(\epsilon) = 0$ due to the absence of an infinite connected cluster. By contrast, when the coordination number is in the range $z_{\mathrm{cond}} < z < z_0$, a network only develops a nonzero differential bulk modulus for positive strains above a threshold $\epsilon_c(z)$. For superisostatic coordination numbers $z > z_0$, the differential bulk modulus is larger than zero in the small strain limit; B increases with ϵ until it reaches a plateau of the large strain limit (see right panels in Figs. 5 and 7).

In contrast to the positive strains, for negative values of the strain, the modulus $B(z,\epsilon)$ of superisostatic networks decreases with $|\epsilon|$ until it vanishes below a threshold, predicted by the nonlinear EM theory in Eq. (B3) (see left plots in Figs. 5, 7, and 8). This collapse was observed for perfect two-dimensional triangular network in Monte Carlo simulations at low temperatures [35,36]. Here, we show that reduction of the mean coordination number shifts this collapse toward smaller values of $|\epsilon|$.

The agreement with the numerical data is good far from the transition point. The bulk modulus in the infinite strain limit

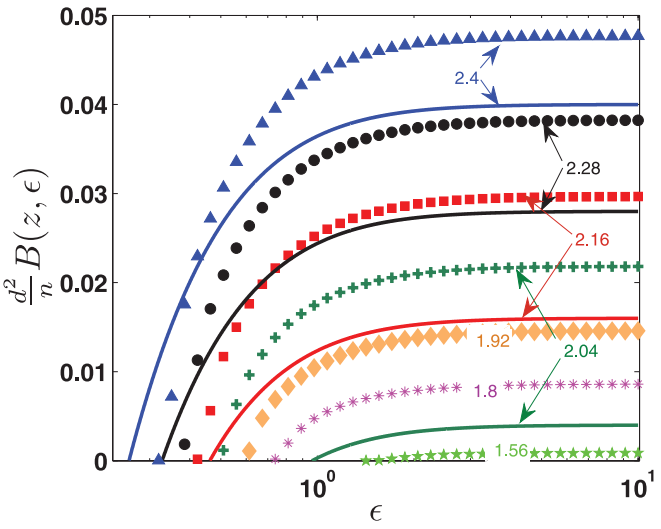

FIG. 6. (Color online) The nonlinear bulk modulus for the diluted fcc lattice as a function of the applied strain for different values of the average coordination number shown as labels next to the curves. The numerical data are depicted as symbols and the nonlinear EM theory predictions are shown as solid lines. For $z < 2$, the EM theory predicts zero bulk modulus for any strain.

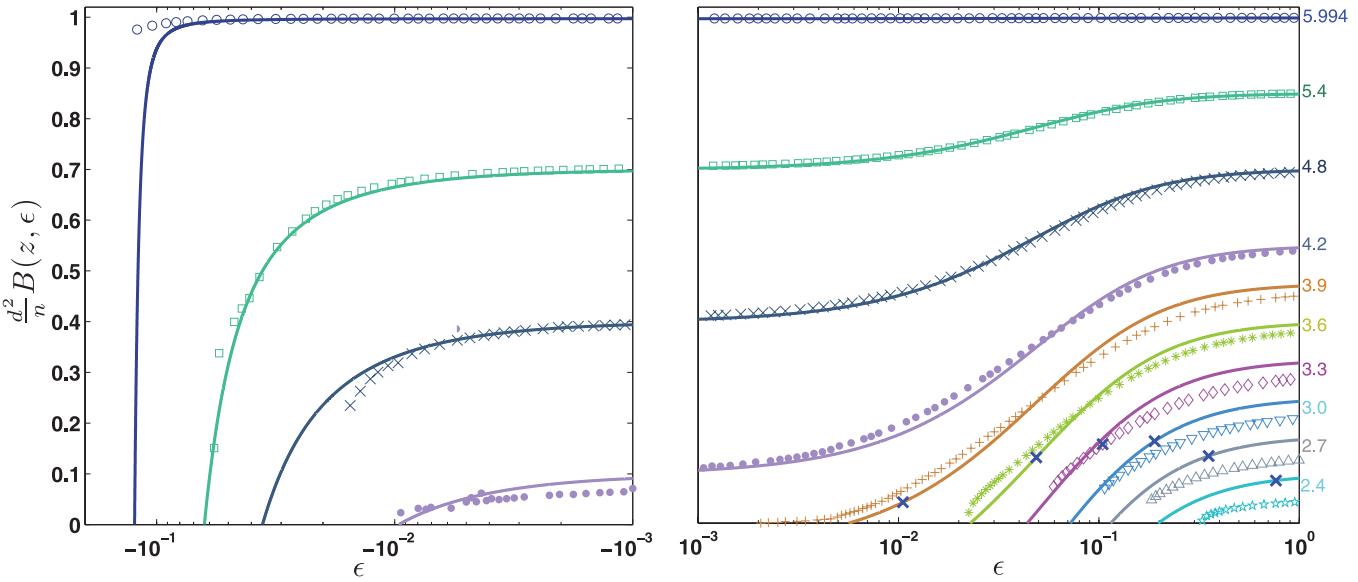

FIG. 7. (Color online) The nonlinear bulk modulus for the diluted triangular lattice as a function of the applied strain for different values of the average coordination number shown as labels next to the curves. The numerical data are depicted as symbols and the nonlinear EM theory predictions are shown as solid lines. Big crosses represent the location of the first order transition as predicted by Eq. (B2).

is given by

$$B_{\mathrm{EM}}(\epsilon \to \infty) = \mu \frac{n}{d^2} \frac{z-2}{\mathcal{Z}-2}, \tag{50}$$

such that the transition average coordination number approaches the conductivity threshold $z_c(\epsilon \to \infty) = 2$. However, the mean-field prediction for the conductivity threshold deviates from the numerical result [59,60]. This may account for the discrepancy between the nonlinear EM theory prediction and the simulation results close to the conductivity percolation threshold in the large strain regime (see Fig. 6 and large strain values for $d = 3$ in Fig. 8). In fact, we find that for the fcc lattice, the rigidity percolation in the large strain limit occurs at $z_c(\epsilon \to \infty) = z_{\mathrm{cond}} = 1.5 \pm 0.3$. This result is consistent with both the empirical law for the conductivity threshold $z_{\mathrm{cond}} \simeq \frac{d}{d-1}$ [60] and with the numerical result of the fcc lattice conductivity threshold $z_{\mathrm{cond}} \simeq 1.442$ [61].

The results discussed above are summarized in a phase diagram shown in Fig. 8. The curves indicate the transition connectivity number between rigid and floppy phases as a function of applied strain. The explicit formulas may be found in Appendix B for both assumptions about the transition order [see Eqs. (B2) and (B3)]. The strain dependence of the isostatic point we find numerically is reasonably well described by the nonlinear EM theory, as shown in Fig. 8. For the negative strain values at the transition point, only the differential bulk modulus vanishes, but not the stress and the elastic energy; this unambiguously corresponds to a second order transition.

D. Nonaffine fluctuations

Here, we demonstrate the method presented in Secs. III A and III B and analyze the nonaffine fluctuations for the particular case of the diluted regular lattices. Using Eqs. (37) and (38), and the expression for the effective parameter $\widetilde{\mu}(\epsilon)$, Eq. (48), one obtains the expressions for the nonaffinity parameters Γ and $\delta\Gamma$. A comparison between the analytical formula and the numerical calculation is shown in Fig. 9. For superisostatic networks, the numerical results agree well with the nonlinear EM theory predictions. However, on the transition curve, the nonaffinity parameter appears to diverge; this divergence is not captured by the nonlinear EM theory. Further insight in this discrepancy between the EM theory and numerical results over a range of parameters (including the divergences) is gained by analyzing two-point correlation functions.

As discussed in Sec. III C, the mean-field assumption of small fluctuations can be determined self-consistently using the two-point, nearest neighbor correlation function defined in Eq. (40). Based on Eq. (43), one may calculate the nonaffine

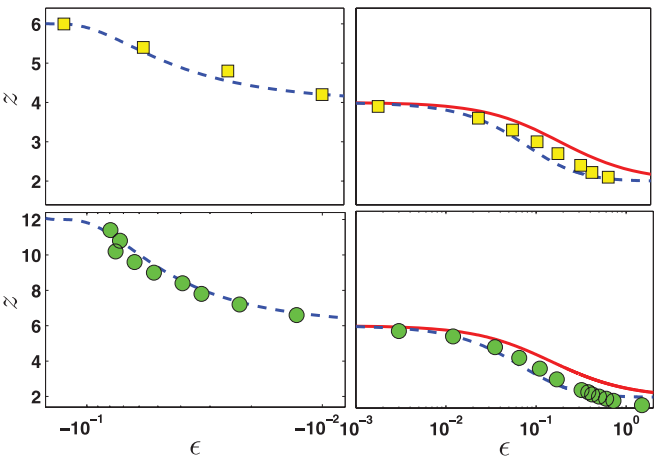

FIG. 8. (Color online) The phase diagram for triangular (upper panels) and fcc (bottom panels) lattices. The numerical data for the transition points are depicted as symbols and the nonlinear EM theory predictions are shown as solid lines for the first order transition given by Eq. (B2) and dashed lines for the second order transition given by Eq. (B3). The curves separate the floppy (below) from the rigid (above) phases.

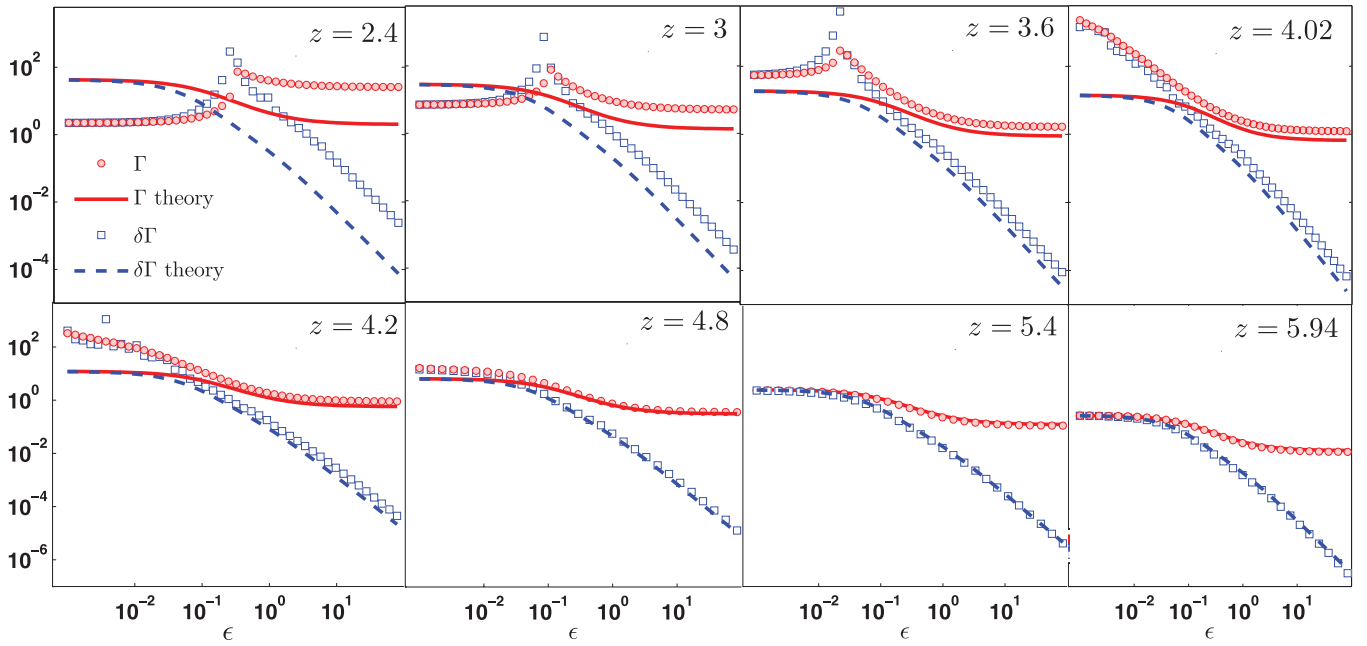

FIG. 9. (Color online) Nonaffinity one-point correlation functions Γ (red filled circles) and $\delta\Gamma$ (blue empty squares) as a function of the applied strain ϵ for different values of the mean coordination number z (see upper right corner of every plot) on the diluted triangular lattice of size 140×140. The lines represent the theoretical prediction for Γ (red solid line) and $\delta\Gamma$ (blue dashed line).

fluctuations $\Gamma_{\rm NN}$ and their differential analog $\delta\Gamma_{\rm NN}$ for the expanded diluted regular networks. The comparison between the theoretical calculation of $\Gamma_{\rm NN}$ and $\delta\Gamma_{\rm NN}$, including the numerical results, is shown in Figs. 10 and 11. The agreement between the theoretical prediction and the numerical data is good when the Ginzburg criterion is satisfied, i.e., $\Gamma_{\rm NN} \ll 1$. Clearly, close to the transition curve, where the nonaffinity parameters diverge, one can expect the EM theory to fail since the Ginzburg criterion is strongly violated. Note, however, that the theoretical prediction for the bulk elastic properties appears to be reasonable even when the Ginzburg criterion is not satisfied (see Figs. 7 and 10 for small values of z).

E. Additional weak interactions: Fiber bending

Many biopolymer networks, including collagen and fibrin networks, have a branched structure with a connectivity close

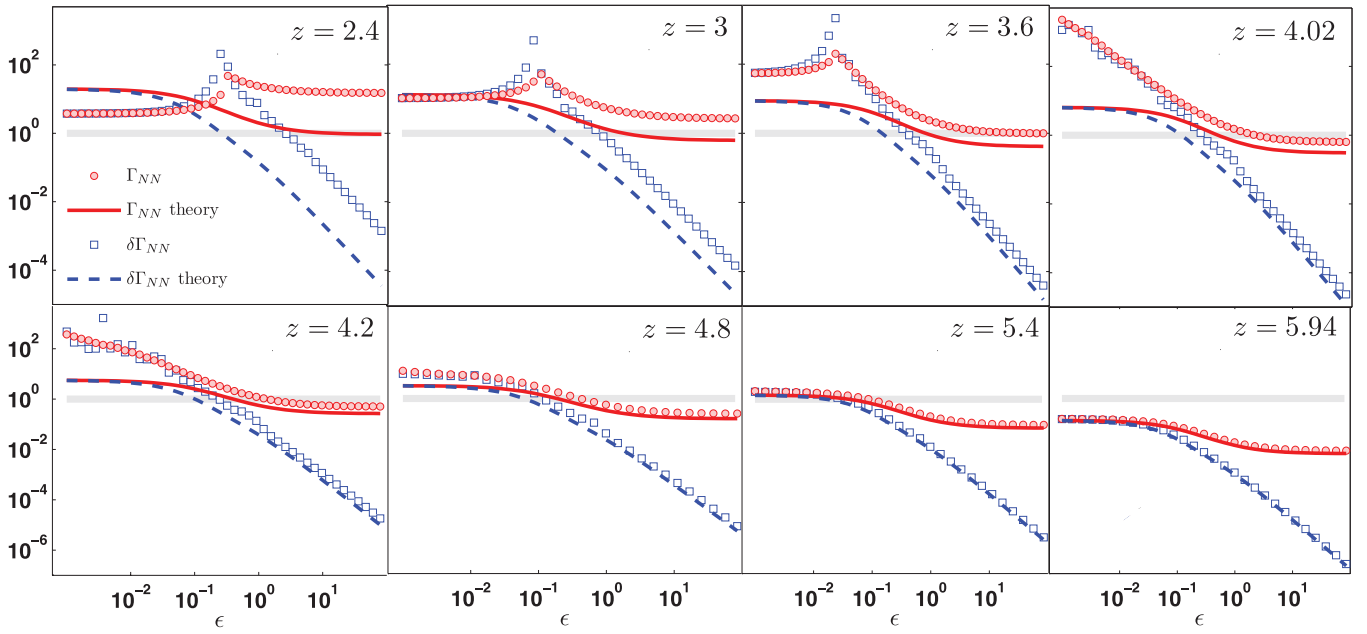

FIG. 10. (Color online) Nonaffinity two-point correlation functions $\Gamma_{\rm NN}$ (red filled circles) and $\delta\Gamma_{\rm NN}$ (blue empty squares) as a function of the applied strain ϵ for different values of the mean coordination number z (see upper right corner of every plot) on the diluted triangular lattice. The lines represent the theoretical prediction for $\Gamma_{\rm NN}$ (red solid line) and $\delta\Gamma_{\rm NN}$ (blue dashed line). The thick gray line indicates the value of 1 to compare with $\Gamma_{\rm NN}$ for the Ginzburg criterion (39).

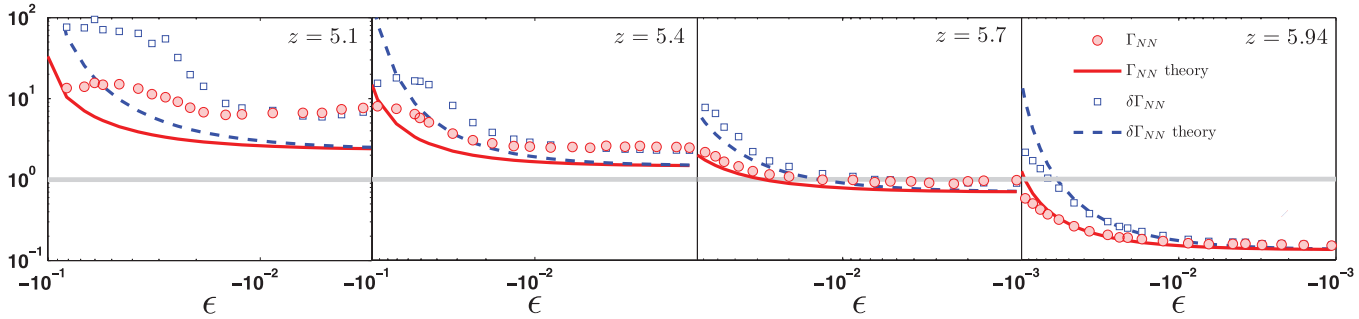

FIG. 11. (Color online) Nonaffinity two-point correlation functions $\Gamma_{\rm NN}$ (red filled circles) and $\delta\Gamma_{\rm NN}$ (blue empty squares) as a function of the *negative* applied strain (compression) ϵ for different values of the mean coordination number z (see upper right corner of every plot) on the diluted triangular lattice. The lines represent the theoretical prediction for $\Gamma_{\rm NN}$ (red solid line) and $\delta\Gamma_{\rm NN}$ (blue dashed line). The thick gray line indicates the value of 1 to compare with $\Gamma_{\rm NN}$ for the Ginzburg criterion (39).

to three on average [40]. The rigidity of such networks with connectivities below Maxwell's central-force isostatic point can be accounted for by the existence of additional non-central-force interactions such as those arising from fiber bending. To analyze the effects of the finite fiber bending stiffness on network elasticity, we generalize the model presented in [34] to the nonlinear regime. The resulting Hamiltonian is composed of two terms representing the stretching and the bending energies:

$$H = \frac{\mu}{2}\sum_{\langle ij\rangle} g_{ij}(|\mathbf{R}_i - \mathbf{R}_j| - 1)^2 + \kappa\sum_{\langle ijk\rangle} g_{ij}g_{jk}(1-\cos\theta_{ijk}), \tag{51}$$

where the summation in the bending term extends over consecutive bonds along the same fiber and $\Delta\theta_{ijk}$ is the angle between the ij and the jk bonds. Here, $g_{ij} = 1$ for uncut bonds (with $\mu_{ij} = \mu$) and $g_{ij} = 0$ for bonds that have been cut (with $\mu_{ij} = 0$). Thus, in this model, the network crosslinks are freely hinging. Various EM theories for this model were developed for the linear elasticity [34,62]. However, the generalization to the nonlinear regime seems to be technically challenging. The nonlinear EM theory described above is used to calculate the nonlinear differential bulk modulus in the $\kappa = 0$ case. To analyze the importance of the additional interactions, we compare our purely central-force, $\kappa = 0$, analytical formula Eqs. (49) and (B1) for the nonlinear bulk modulus to the numerical results for different values of κ (see Fig. 12). For small enough values of κ, the nonlinear bulk modulus does not depend on κ above the central-force isostatic point. By contrast, below the transition strain, $B(\epsilon)$ approaches a plateau proportional to κ, which is not captured by the central-force nonlinear EM theory. However, the strain at which the network exhibits strain stiffening appears to be well approximated by the nonlinear EM theory prediction.

V. BRANCHED NETWORKS AND RANDOM BOND MODEL

The nonlinear EM theory predicts an expression for the bulk modulus [Eq. (49), and more explicitly in Eq. (B1)] for a regular, diluted elastic network that depends on the geometry of the undiluted network only via its coordination number $\mathcal{Z}$. This number sets the maximal possible coordination number of the lattice. In some cases, such as collagen-I that exhibits a branched structure [40], the maximal possible coordination number seems to be very high such that the probability distribution of z is exponential. For such a networks, it is

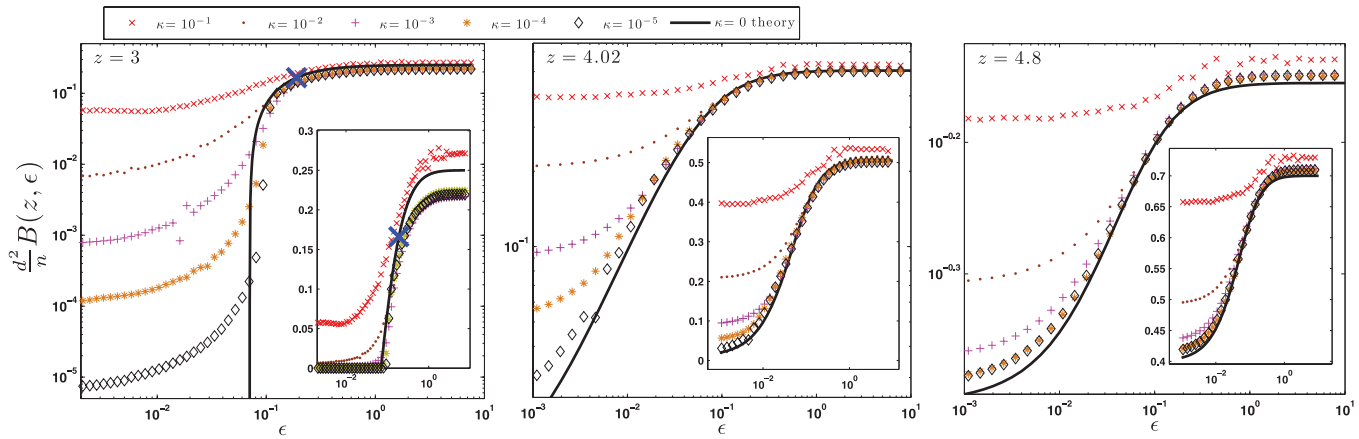

FIG. 12. (Color online) The nonlinear bulk modulus for the triangular lattice as a function of the applied strain for different values of the bending modulus (see legend above the plots). The average coordination numbers are 3, 4.02, and 4.8 (see upper left corner on each plot). The theoretical curves are given by Eq. (49) and, in the explicit form, by Eq. (B1). Insets show the same plots on the semilog scale. Big crosses represent the location of the first order transition as predicted by Eq. (B2)

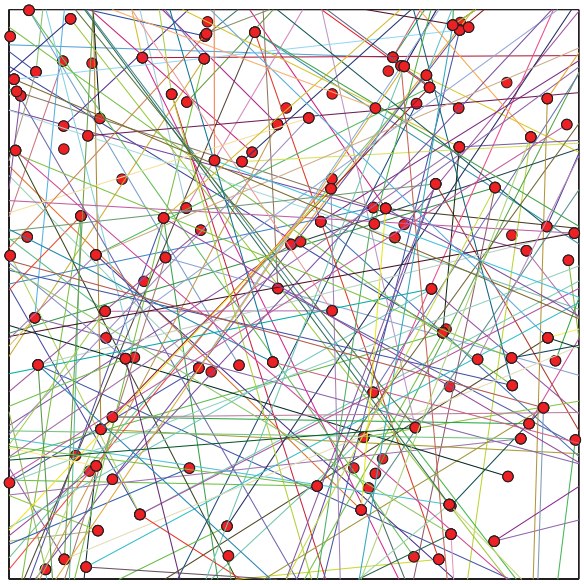

FIG. 13. (Color online) Illustration of the random bond model network in two dimensions. Here, the density of the bonds is $n_d = 1/3$ and the mean coordination number is $z = 2$.

instructive to consider a high $\mathcal{Z}$ limit of the expression for the bulk modulus Eqs. (49) or (B1). More specifically, an effectively off-lattice network with an exponentially distributed coordination number with a given mean

$$z = \mathcal{P}\mathcal{Z} \tag{52}$$

can be constructed by almost total dilution $\mathcal{P} \to 0$ of a highly coordinated undiluted regular lattice $\mathcal{Z} \to \infty$. A particularly simple example of this type of network is the random bond model where randomly located points are randomly connected [63,64] (see Fig. 13). Using this limiting procedure, the expressions for the bulk modulus reduce to

$$B_{\mathrm{EM}}(z,\epsilon) = \frac{n_d}{zd^2}\left(z - 2 - \frac{d-1}{d+2}\left\{\frac{2(d+1)}{[1+(2+d)\epsilon]^3} - \frac{6}{\left(1+\frac{d+2}{3}\epsilon\right)^3}\right\}\right), \tag{53}$$

where n_d is the density of the bonds of the diluted network. The transition curve is given by

$$z_c(\epsilon) = 2 + \frac{d-1}{d+2}\left\{\frac{2\,(d+1)}{[1+(2+d)\,\epsilon]^3} - \frac{6}{\left(1+\frac{d+2}{3}\epsilon\right)^3}\right\}. \tag{54}$$

These results may be directly applied to the random bond model. A comparison between the numerical calculation of the random bond model bulk modulus and Eq. (53) for $d = 2$ is shown in Fig. 14. Branched networks with exponential distribution of the local connectivity are also expected to behave according to Eq. (53).

VI. SUMMARY AND DISCUSSION

Motivated by the rich nonlinear elastic behavior of disordered materials, we studied random spring networks under isotropic strains. We provided a quantitative analytical theory for the strain-stiffening phenomena that are driven by nonuniform (nonaffine) deformation fields originating in the network disorder. We considered disordered networks on lattice topologies of Hookean springs. The disorder is introduced with a nonuniform distribution of the spring constants for the bonds on a regular lattice. The central parameter that characterizes such networks is the mean coordination number z; the threshold $z = z_c$ separates a floppy from a rigid phase. However, when some fraction of the bonds are under stress, the isostatic coordination number can shift continuously to lower values [52]. This can be realized, for example, by applying a large deformation to the network [7] or by introducing local contractile forces [46]. It was shown that rigidity can be induced by additional stresses or strains in networks with connectivities below the zero strain isostatic point $z_0 = z_c\,(\epsilon \to 0) = 2d$ in d dimensions. As a result, a significant strain stiffening is induced as the network transitions from the floppy to the rigid phase.

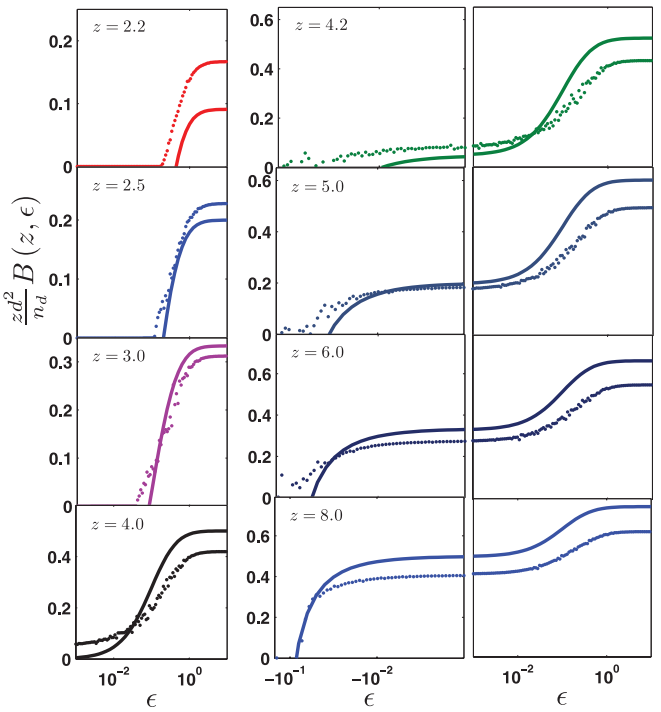

FIG. 14. (Color online) The differential nonlinear bulk modulus as a function of the applied strain of the two-dimensional random bond model network for different values of the mean coordination number z. The dots represent the numerical result, while the solid lines are based on Eq. (53).

Here, we have developed a nonlinear effective medium approach for regular central-force networks with disordered spring constants to provide insight in such behavior. In this model, we expand the Hamiltonian around the affine deformation state for an isotropically expanded network. Thus, this theory explicitly accounts for nonaffine deformations that are small compared to the affinely strained unit cell. The main result of the EM theory approach is the nonlinear differential bulk modulus given by Eq. (49), where the effective parameter $\tilde{\mu}$ may be found for a given spring constant probability density of the original network $P(\mu_{ij})$ using

Eq. (18). We demonstrated that this theory quantitatively captures the nonlinear elastic properties of a bond-diluted network for arbitrary strains far from a transition in two and three dimensions. In particular, this theory predicts a continuous transition curve for the strain-dependent isostatic point, varying from $z_0 = z_c\,(\epsilon \to 0) \simeq 2d$ at zero strain to the conductivity threshold $z_{\rm cond} \simeq 2$ in the infinite strain limit. The transition at the strain-dependent rigidity point is accompanied with divergent strain fluctuations, reminiscent of critical behavior. We showed how the nonlinear EM theory can be used to calculate the correlation functions associated to such strain fluctuations. The two-point nonaffinity parameter, quantifying the relative nonaffine deformations of neighboring points, can be used to inspect internal consistency (Ginzburg criterion) of the nonlinear EM theory approach, which breaks down in the vicinity of the (strain-dependent) rigidity percolation point.

Application of the EM theory developed here presupposes that the order of the transition is known. From our numerical results, one can not rule out the possibility of either a first or a second order transition. This remains a subject of further study [48].

We found that a superisostatic disordered network with $z > 2d$ may lose rigidity under positive pressure (negative strain values) in two- and three-dimensional networks. Similar elastic collapse was found and analyzed for the perfect triangular lattice[2] [35,36]. Here, we showed that the location of such a collapse depends mostly on the network topology via the mean coordination number. The mean-field approach developed here is found to predict reasonably well the location of the collapse and the elastic properties of the network for the negative strain values.

We also investigated the effects of additional weak non-central-force interactions numerically in the form of fiber bending in bond-diluted networks. The resulting fiber network exhibits a strain-stiffening transition from a soft, bending-dominated regime to a stretching-dominated regime. Importantly, however, this transition still occurs at the transition strain predicted by the central-force nonlinear EM theory, which quantitatively captures the nonlinear elasticity beyond the transition strain. These results may lend insight into the nonlinear elasticity of biological fiber networks.

The EM theory expressions for the elasticity behavior of random spring networks depend on the network geometry only via the coordination number of the undiluted network $\mathcal{Z}$. One may interpret $\mathcal{Z}$ also as the maximal coordination number of the diluted network. This may lead to the temptation to use the results obtained here for other than diluted regular network systems, including networks with geometrical disorder. However, there is at least one example where a network based on the jammed configuration geometry has qualitatively different elastic behavior than the diluted regular network with the same mean coordination number [65]. In this work, we defined the strain of the diluted network relative to the zero energy state of the undiluted network. Therefore, it is unclear how our results may be extrapolated for geometrically disordered networks. Nevertheless, we have shown that our results may be applied to describe the elastic response of the geometrically disordered random bond model.

In this work, we focused on the differential *bulk* modulus of networks under strain. However, for many experimentally relevant systems, the *shear* and the *Young's* moduli may be more relevant. To investigate such systems, a generalization of the nonlinear EM theory presented here to anisotropic deformations is required. This appears to be technically challenging and will be an interesting subject of further study, along with the order of the transition, transition behavior, and various consequences of geometrical and topological disorder.

[2]In contrast to Refs. [35,36] we discuss in this paper only uniform deformations. Therefore, in our case the collapse can occur only under compressional deformation.

ACKNOWLEDGMENTS

This work was funded by FOM/NWO and by National Science Foundation under Grant No. NSF PHY05-51164. We thank M. Rubinshtein, M. Das, C. Heusinger, and L. Jawerth for fruitful discussions. We also thank X. Mao and T. C. Lubensky for discussions and for sharing their related work [66].

APPENDIX A: CALCULATION OF $\tilde{\mu}_{\rm EM}$

In this appendix, we calculate $\mu_{\rm EM}$, the displacement of the *nm* bond in the *unperturbed* EM network due to a unit force $\mathbf{r}_{nm}$ acting on the *nm* bond. The dynamical matrix of the unperturbed EM Hamiltonian (12) is given by

$$D_{ij} = \begin{cases} -\frac{\tilde{\mu}}{1+\epsilon}(\mathbf{r}_{ij} \otimes \mathbf{r}_{ij} + \epsilon \mathbb{1}), & i \neq j \\ \frac{\tilde{\mu}}{1+\epsilon}\sum_{j \neq i}(\mathbf{r}_{ij} \otimes \mathbf{r}_{ij} + \epsilon \mathbb{1}), & i = j \end{cases} \tag{A1}$$

where $\mathbb{1}$ is the unit tensor and $\otimes$ is the external product. The Fourier transform of D is given by

$$D(\mathbf{k}) = \sum_{ij} D_{ij} e^{i\mathbf{k}\cdot\mathbf{r}_{ij}} = \frac{\tilde{\mu}}{1+\epsilon}\sum_{\mathbf{r}}(\mathbf{r} \otimes \mathbf{r} + \epsilon \mathbb{1})(1 - e^{i\mathbf{k}\cdot\mathbf{r}}), \tag{A2}$$

where $\mathbf{r}$ runs over all unit bond vectors. The unit force acting on the *nm* bond is given by

$$\mathbf{f}_i = \mathbf{r}_{nm}(\delta_{i,n} - \delta_{i,m}), \tag{A3}$$

so that its Fourier transform is

$$\mathbf{f}(\mathbf{k}) = \sum_i \mathbf{f}_i e^{i\mathbf{k}\cdot\mathbf{R}_i} = \mathbf{r}_{nm}(1 - e^{i\mathbf{k}\cdot\mathbf{r}_{nm}}). \tag{A4}$$

Thus, the Fourier transform of the displacement field is given by

$$\mathbf{v}\,(\mathbf{k}) = -D^{-1}\,(\mathbf{k}) \cdot \mathbf{f}\,(\mathbf{k})\,. \tag{A5}$$

The displacement of the nm bond due to the unit force is

$$\frac{1}{\mu_{\rm EM}} = \mathbf{r}_{nm}\cdot\sum_{\mathbf{k}}\mathbf{v}(\mathbf{k})(e^{-i\mathbf{k}\cdot\mathbf{r}_{nm}}-1) = -\sum_{\mathbf{k}}\mathbf{r}_{nm}\cdot\mathbf{f}(\mathbf{k})D^{-1}(\mathbf{k})(e^{-i\mathbf{k}\cdot\mathbf{r}_{nm}}-1)$$
$$= \frac{1}{\widetilde{\mu}}\frac{2d(1+\epsilon)}{\mathcal{Z}}\left[1-\frac{\epsilon}{d}\sum_{\mathbf{k}}\mathrm{Tr}\left\{\frac{\sum_{\mathbf{r}}(1-e^{i\mathbf{k}\cdot\mathbf{r}})}{\sum_{\mathbf{r}}(\mathbf{r}\otimes\mathbf{r}+\epsilon\mathbb{1})(1-e^{i\mathbf{k}\cdot\mathbf{r}})}\right\}\right]\equiv\frac{a(\epsilon)}{\widetilde{\mu}}. \tag{A6}$$

For a highly coordinated lattice, the sum over $\mathbf{r}$ may be well approximated by the integral over the sphere that includes all the neighboring crosslinks and, since the sum over $\mathbf{k}$ is dominated by the small $\mathbf{k}\cdot\mathbf{r}\ll\mathbf{1}$ values, $a(\epsilon)$ may be approximated by

$$a(\epsilon)\simeq\frac{2d\,(1+\epsilon)}{\mathcal{Z}}\left[1-\frac{\epsilon}{d}\mathrm{Tr}\left\{\frac{\oint(\mathbf{k}\cdot\mathbf{r})^2d^{d-1}\mathbf{r}}{\oint(\mathbf{k}\cdot\mathbf{r})^2d^{d-1}\mathbf{r}(\mathbf{r}\otimes\mathbf{r}+\epsilon\mathbb{1})}\right\}\right]=\frac{2d(1+\epsilon)}{\mathcal{Z}}\left[1-\frac{\epsilon}{d}\left(\frac{1}{\frac{3}{2+d}+\epsilon}+\frac{d-1}{\frac{1}{2+d}+\epsilon}\right)\right]. \tag{A7}$$

APPENDIX B: EXPLICIT RESULTS FOR DILUTED NETWORKS

In this appendix, we present the explicit results for diluted networks. The nonlinear differential bulk modulus calculated using (49) is given by

$$B_{\rm EM}(\epsilon,z) = \frac{n}{d^2}\frac{\mu}{\{(d+2)^2(\mathcal{Z}-2)\epsilon^2-2[d^2+7d-2(d+2)\mathcal{Z}+4]\epsilon-6d+3\mathcal{Z}\}^3}$$
$$\times\left\{\begin{array}{l}
\epsilon^3((z-2)\epsilon\{(\mathcal{Z}-2)\epsilon[(\mathcal{Z}-2)\epsilon-6]+12\}-8)d^6\\
+2\epsilon^2[6(z-2)(\mathcal{Z}-2)^2\epsilon^4+3(z-2)(\mathcal{Z}-2)(2\mathcal{Z}-15)\epsilon^3]d^5\\
+2\epsilon^2[-3(z-2)(11\mathcal{Z}-42)\epsilon^2+4(14z+\mathcal{Z}-39)\epsilon-36]d^5\\
+\epsilon\{60(z-2)(\mathcal{Z}-2)^2\epsilon^5+24(z-2)(\mathcal{Z}-2)(5\mathcal{Z}-21)\epsilon^4+3(z-2)[\mathcal{Z}(19\mathcal{Z}-262)+564]\epsilon^3\}d^4\\
+\epsilon\{-2[(\mathcal{Z}-334)\mathcal{Z}+z(137\mathcal{Z}-626)+1428]\epsilon^2+72(5z+\mathcal{Z}-17)\epsilon-216\}d^4\\
+2[80(z-2)(\mathcal{Z}-2)^2\epsilon^6+24(z-2)(\mathcal{Z}-2)(10\mathcal{Z}-29)\epsilon^5]d^3\\
+2\{12(z-2)[\mathcal{Z}(19\mathcal{Z}-140)+206]\}\epsilon^4+[(2398-167\mathcal{Z})\mathcal{Z}]d^3\\
+2\{z[\mathcal{Z}(68\mathcal{Z}-1063)+2198]-4636\}\epsilon^3-9[(\mathcal{Z}-94)\mathcal{Z}]d^3\\
+2\{[(29\mathcal{Z}-114)+276]\epsilon^2+108(2z+\mathcal{Z}-7)\epsilon-108\}d^3\\
+\{240(z-2)(\mathcal{Z}-2)^2\epsilon^6+96(z-2)(\mathcal{Z}-2)(10\mathcal{Z}-21)\epsilon^5+24(z-2)[\mathcal{Z}(57\mathcal{Z}-274)+282]\epsilon^4\}d^2\\
+(9\{12(51-5\mathcal{Z})\mathcal{Z}+z[19(\mathcal{Z}-14)\mathcal{Z}+336]-544\}\epsilon^2-54[8z(\mathcal{Z}-2)+(\mathcal{Z}-28)\mathcal{Z}+16]\epsilon+108(z+2\mathcal{Z}))d^2\\
+(8\{5(286-45\mathcal{Z})\mathcal{Z}+z[3\mathcal{Z}(34\mathcal{Z}-231)+742]-1428\}\epsilon^3)d^2\\
+2\{(96(z-2)(\mathcal{Z}-2)^2\epsilon^6+240(z-2)[\mathcal{Z}(2\mathcal{Z}-7)+6]\epsilon^5\}d\\
+2\{48(z-2)(\mathcal{Z}-1)(19\mathcal{Z}-42)\epsilon^4+4[(1262-407\mathcal{Z})\mathcal{Z}]\}d\\
+2\{z[\mathcal{Z}(204\mathcal{Z}-679)+334]-624\}\epsilon^3+18\{z[\mathcal{Z}(19\mathcal{Z}-80)+20]\}d\\
+2\{[-2(3\mathcal{Z}-8)(7\mathcal{Z}-2)]\epsilon^2+27[2z(\mathcal{Z}-8)-7\mathcal{Z}+16]\mathcal{Z}\epsilon-27\mathcal{Z}(2z+\mathcal{Z})\}d\\
+z(64\{4\epsilon[\epsilon(\epsilon+3)+3]+5\}\epsilon^3-8\mathcal{Z}(4\epsilon\{\epsilon[4\epsilon(2\epsilon+9)+57]+41\}+45)\epsilon^2+\mathcal{Z}^2[4\epsilon(\epsilon+2)+3]^3)\\
-8\epsilon\big[64\epsilon^2(\epsilon+1)^3-8\mathcal{Z}\epsilon(\epsilon\{\epsilon[4\epsilon(2\epsilon+9)+57]+37\}+9)+\mathcal{Z}^2\big(2\epsilon(2\epsilon\{\epsilon[4\epsilon(\epsilon+6)+57]+61\}+63)+27\big)\big]
\end{array}\right\} \tag{B1}$$

for $\epsilon>\epsilon_c$. Below the transition curve, the nonlinear differential bulk modulus vanishes. The transition curve for the assumption of the first order transition is given by

$$z_{c_1}(\epsilon)=\frac{\left\{\begin{array}{l}18d(-2d+\mathcal{Z})+3\{-8d[4+d(7+d)]+[12+d(29+7d)]\mathcal{Z}\}\epsilon\\-4(16+d\{80+d[81+d(20+d-2\mathcal{Z})-21\mathcal{Z}]-48\mathcal{Z}\}-28\mathcal{Z})\epsilon^2\\+(2+d)^2\{-8[4+d(7+d)]+[28+d(19+d)]\mathcal{Z}\}\epsilon^3+2(2+d)^4(-2+\mathcal{Z})\epsilon^4\end{array}\right\}}{\left\{\begin{array}{l}9(-2d+\mathcal{Z})-3[4+31d+13d^2-8(2+d)\mathcal{Z}]\epsilon-2(2+d)\{2[8+5d(4+d)]-11(2+d)\mathcal{Z}\}\epsilon^2\\-(2+d)^2[20+25d+3d^2-8(2+d)\mathcal{Z}]\epsilon^3+(2+d)^4(-2+\mathcal{Z})\epsilon^4\end{array}\right\}}. \tag{B2}$$

The transition curve for the assumption of the second order transition is given by

$$z_{c_2}(\epsilon)=2\frac{\left\{\begin{array}{l}(d+2)^6(\mathcal{Z}-2)^2\epsilon^6-6(d+2)^4(\mathcal{Z}-2)[d^2+7d-2(d+2)\mathcal{Z}+4]\epsilon^5\\+3(d+2)^2(19(d+2)^2\mathcal{Z}^2-2(d+2)[d(11d+65)+38]\mathcal{Z}+4\{d(d+4)[d(d+13)+17]+16\})\epsilon^4\\+((d+2)^2[d(d+163)+244]\mathcal{Z}^2-2(d+2)(d\{d[d(2d+163)+873]+1114\}+296)\mathcal{Z})\epsilon^3\\+\big(4[d(d+7)+4](d\{d[d(d+32)+129]+128\}+16)\big)\epsilon^3\\+9(2d-\mathcal{Z})\big(2\{d(d+4)[d(d+13)+17]+16\}-(d+2)[d(d+28)+28]\mathcal{Z}\big)\epsilon^2\\+27[d(d+7)+4](\mathcal{Z}-2d)^2\epsilon+27d(\mathcal{Z}-2d)^2\end{array}\right\}}{\left\{\begin{array}{l}(d+2)^6(\mathcal{Z}-2)^2\epsilon^6-6(d+2)^4(\mathcal{Z}-2)[d^2+7d-2(d+2)\mathcal{Z}+4]\epsilon^5\\+3(d+2)^2(19(d+2)^2\mathcal{Z}^2-2(d+2)[d(11d+65)+38]\mathcal{Z}+4\{d(d+4)[d(d+13)+17]+16\})\epsilon^4\\+2(d+2)\{68(d+2)^2\mathcal{Z}^2-(d+2)[d(137d+515)+164]\mathcal{Z}+2d[d(d+5)(28d+117)+314]+80\}\epsilon^3\\+9(d+2)[d(20d-19\mathcal{Z}+74)-38\mathcal{Z}+20](2d-\mathcal{Z})\epsilon^2+108(d+2)(\mathcal{Z}-2d)^2\epsilon+27(\mathcal{Z}-2d)^2\end{array}\right\}}. \tag{B3}$$

APPENDIX C: CALCULATION OF THE DIFFERENTIAL NONAFFINITY PARAMETER

The only unknown term in the differential nonaffinity expression in Eq. (38) is $\langle(\frac{d\mathbf{v}_n(\epsilon)}{d\epsilon})^2\rangle$. This term may be evaluated within the framework of the EM theory as follows. Using Eqs. (26), (27), and (30), one obtains

$$\left\langle\left(\frac{d\mathbf{v}_n(\epsilon)}{d\epsilon}\right)^2\right\rangle=\frac{1}{2N^2}\sum_{\mathbf{r},\mathbf{k}}\left\{\begin{array}{l}\left\langle\left\{\frac{d}{d\epsilon}\left[\frac{\epsilon(1+\epsilon)}{a(\epsilon)}\frac{\widetilde{\mu}-\mu_{ij}}{\frac{\widetilde{\mu}}{a(\epsilon)}-\widetilde{\mu}+\mu_{ij}}\right]\right\}^2\right\rangle\frac{(1-e^{i\mathbf{k}\cdot\mathbf{r}})}{\sum_{\mathbf{r}}(\mathbf{r}\otimes\mathbf{r}+\epsilon\mathbb{1})(1-e^{i\mathbf{k}\cdot\mathbf{r}})}\mathbf{r}\frac{(1-e^{-i\mathbf{k}\cdot\mathbf{r}})}{\sum_{\mathbf{r}}(\mathbf{r}\otimes\mathbf{r}+\epsilon\mathbb{1})(1-e^{-i\mathbf{k}\cdot\mathbf{r}})}\mathbf{r}\\-\left\langle\frac{d}{d\epsilon}\left[\frac{\epsilon(1+\epsilon)}{a(\epsilon)}\frac{\widetilde{\mu}-\mu_{ij}}{\frac{\widetilde{\mu}}{a(\epsilon)}-\widetilde{\mu}+\mu_{ij}}\right]^2\right\rangle\frac{(1-e^{i\mathbf{k}\cdot\mathbf{r}})}{\sum_{\mathbf{r}}(\mathbf{r}\otimes\mathbf{r}+\epsilon\mathbb{1})(1-e^{i\mathbf{k}\cdot\mathbf{r}})}\mathbf{r}\frac{(1-e^{-i\mathbf{k}\cdot\mathbf{r}})\sum_{\mathbf{r}'}(1-e^{-i\mathbf{k}\cdot\mathbf{r}'})}{\left[\sum_{\mathbf{r}}(\mathbf{r}\otimes\mathbf{r}+\epsilon\mathbb{1})(1-e^{-i\mathbf{k}\cdot\mathbf{r}})\right]^2}\mathbf{r}\\+\left\langle\left[\frac{\epsilon(1+\epsilon)}{a(\epsilon)}\frac{\widetilde{\mu}-\mu_{ij}}{\frac{\widetilde{\mu}}{a(\epsilon)}-\widetilde{\mu}+\mu_{ij}}\right]^2\right\rangle\frac{(1-e^{i\mathbf{k}\cdot\mathbf{r}})\sum_{\mathbf{r}'}(1-e^{-i\mathbf{k}\cdot\mathbf{r}'})}{\left[\sum_{\mathbf{r}}(\mathbf{r}\otimes\mathbf{r}+\epsilon\mathbb{1})(1-e^{i\mathbf{k}\cdot\mathbf{r}})\right]^2}\mathbf{r}\frac{(1-e^{-i\mathbf{k}\cdot\mathbf{r}})\sum_{\mathbf{r}'}(1-e^{-i\mathbf{k}\cdot\mathbf{r}'})}{\left[\sum_{\mathbf{r}}(\mathbf{r}\otimes\mathbf{r}+\epsilon\mathbb{1})(1-e^{-i\mathbf{k}\cdot\mathbf{r}})\right]^2}\mathbf{r}\end{array}\right\}. \tag{C1}$$

As before, we apply the approximation of the highly coordinated lattice and get

$$\left\langle\left(\frac{d\mathbf{v}_n(\epsilon)}{d\epsilon}\right)^2\right\rangle=\frac{d}{2\mathcal{Z}}A_d f_d(N)\left\{\begin{array}{l}\left\langle\left\{\frac{d}{d\epsilon}\left[\frac{\epsilon(1+\epsilon)}{a(\epsilon)}\frac{\widetilde{\mu}-\mu_{ij}}{\frac{\widetilde{\mu}}{a(\epsilon)}-\widetilde{\mu}+\mu_{ij}}\right]\right\}^2\right\rangle\left\{\frac{\frac{3}{2+d}}{\left(\frac{3}{2+d}+\epsilon\right)^2}+\frac{\frac{d-1}{2+d}}{\left(\frac{1}{2+d}+\epsilon\right)^2}\right\}\\-\frac{d}{d\epsilon}\left\langle\left[\frac{\epsilon(1+\epsilon)}{a(\epsilon)}\frac{\widetilde{\mu}-\mu_{ij}}{\frac{\widetilde{\mu}}{a(\epsilon)}-\widetilde{\mu}+\mu_{ij}}\right]^2\right\rangle\left\{\frac{\frac{3}{2+d}}{\left(\frac{3}{2+d}+\epsilon\right)^3}+\frac{\frac{d-1}{2+d}}{\left(\frac{1}{2+d}+\epsilon\right)^3}\right\}\\+\left\langle\left[\frac{\epsilon(1+\epsilon)}{a(\epsilon)}\frac{\widetilde{\mu}-\mu_{ij}}{\frac{\widetilde{\mu}}{a(\epsilon)}-\widetilde{\mu}+\mu_{ij}}\right]^2\right\rangle\left\{\frac{\frac{3}{2+d}}{\left(\frac{3}{2+d}+\epsilon\right)^4}+\frac{\frac{d-1}{2+d}}{\left(\frac{1}{2+d}+\epsilon\right)^4}\right\}\end{array}\right\} \tag{C2}$$

[1] A. J. Liu and S. R. Nagel, Nature (London) **396**, 21 (1998).
[2] M. E. Cates, J. P. Wittmer, J. P. Bouchaud, and P. Claudin, Phys. Rev. Lett. **81**, 1841 (1998).
[3] A. R. Bausch and K. Kroy, Nat. Phys. **2**, 231 (2006).
[4] K. E. Kasza, A. C. Rowat, J. Liu, T. E. Angelini, C. P. Brangwynne, G. H. Koenderink, and D. A. Weitz, Curr. Opin. Cell Biol. **19**, 101 (2007).
[5] D. A. Fletcher and R. D. Mullins, Nature (London) **463**, 485 (2010).
[6] C. S. O'Hern, L. E. Silbert, A. J. Liu, and S. R. Nagel, Phys. Rev. E **68**, 011306 (2003).
[7] M. Wyart, H. Liang, A. Kabla, and L. Mahadevan, Phys. Rev. Lett. **101**, 215501 (2008).
[8] M. van Hecke, J. Phys.: Condens. Matt. **22**, 033101 (2010).
[9] A. J. Liu, S. R. Nagel, W. van Saarloos, and M. Wyart, e-print arXiv:1006.2365.
[10] P. A. Janmey, U. Euteneuer, P. Traub, and M. Schliwa, J. Cell Biol. **113**, 155 (1991).
[11] M. L. Gardel, J. H. Shin, F. C. MacKintosh, L. Mahadevan, P. Matsudaira, and D. A. Weitz, Science **304**, 1301 (2004).
[12] C. Storm, J. J. Pastore, F. C. MacKintosh, T. C. Lubensky, and P. A. Janmey, Nature (London) **435**, 191 (2005).
[13] O. Lieleg, M. Claessens, C. Heussinger, E. Frey, and A. R. Bausch, Phys. Rev. Lett. **99**, 088102 (2007).
[14] R. E. Shadwick, J. Exp. Biol. **202**, 3305 (1999).
[15] J. P. Winer, S. Oake, and P. A. Janmey, PLoS One **4**, e6382 (2009).
[16] P. R. Onck, T. Koeman, T. van Dillen, and E. Van der Giessen, Phys. Rev. Lett. **95**, 178102 (2005).
[17] M. L. Gardel, F. Nakamura, J. H. Hartwig, J. C. Crocker, T. P. Stossel, and D. A. Weitz, Proc. Natl. Acad. Sci. USA **103**, 1762 (2006).

[18] B. Wagner, R. Tharmann, I. Haase, M. Fischer, and A. R. Bausch, Proc. Natl. Acad. Sci. USA **103**, 13974 (2006).
[19] E. M. Huisman, T. van Dillen, P. R. Onck, and E. Van der Giessen, Phys. Rev. Lett. **99**, 208103 (2007).
[20] C. Heussinger, B. Schaefer, and E. Frey, Phys. Rev. E **76**, 031906 (2007).
[21] O. Chaudhuri, S. H. Parekh, and D. A. Fletcher, Nature (London) **445**, 295 (2007).
[22] C. P. Broedersz, C. Storm, and F. C. MacKintosh, Phys. Rev. Lett. **101**, 118103 (2008).
[23] K. E. Kasza, G. H. Koenderink, Y. C. Lin, C. P. Broedersz, W. Messner, F. Nakamura, T. P. Stossel, F. C. MacKintosh, and D. A. Weitz, Phys. Rev. E **79**, 041928 (2009).
[24] E. Conti and F. C. MacKintosh, Phys. Rev. Lett. **102**, 088102 (2009).
[25] P. A. Janmey, M. E. McCormick, S. Rammensee, J. L. Leight, P. C. Georges, and F. C. MacKintosh, Nat. Mater. **6**, 48 (2007).
[26] J. D. Bernal and J. Mason, Nature (London) **188**, 910 (1960).
[27] A. Kabla and L. Mahadevan, J. R. Soc., Int. **4**, 99 (2007).
[28] D. T. N. Chen, Q. Wen, P. A. Janmey, J. C. Crocker, and A. G. Yodh, Annu. Rev. Condens. Matter Phys. **1**, 301 (2010).
[29] W. Tang and M. F. Thorpe, Phys. Rev. B **37**, 5539 (1988).
[30] J. C. Maxwell, Philos. Mag. **27**, 294 (1864).
[31] M. F. Thorpe, J. Non-Cryst. Solids **57**, 355 (1983).
[32] S. Feng and P. N. Sen, Phys. Rev. Lett. **52**, 216 (1984).
[33] D. J. Jacobs and M. F. Thorpe, Phys. Rev. E **53**, 3682 (1996).
[34] C. P. Broedersz, X. Mao, T. C. Lubensky, and F. C. MacKintosh, Nature Physics **7**, 983 (2011).
[35] D. E. Discher, D. H. Boal, and S. K. Boey, Phys. Rev. E **55**, 4762 (1997).
[36] W. Wintz, R. Everaers, and U. Seifert, J. Phys. I **7**, 1097 (1997).
[37] F. C. MacKintosh, J. Kas, and P. A. Janmey, Phys. Rev. Lett. **75**, 4425 (1995).
[38] Y. C. Lin, N. Y. Yao, C. P. Broedersz, H. Herrmann, F. C. MacKintosh, and D. A. Weitz, Phys. Rev. Lett. **104**, 58101 (2010).
[39] A. M. Stein, D. A. Vader, D. A. Weitz, and L. M. Sander, Complexity **16**, 22 (2010).
[40] S. B. Lindstrom, D. A. Vader, A. Kulachenko, and D. A. Weitz, Phys. Rev. E **82**, 051905 (2010).
[41] J. Wilhelm and E. Frey, Phys. Rev. Lett. **91**, 108103 (2003).
[42] D. A. Head, A. J. Levine, and F. C. MacKintosh, Phys. Rev. E **68**, 061907 (2003).
[43] D. A. Head, A. J. Levine, and F. C. MacKintosh, Phys. Rev. Lett. **91**, 108102 (2003).
[44] C. Heussinger, M. Bathe, and E. Frey, Phys. Rev. Lett. **99**, 048101 (2007).
[45] T. van Dillen, P. R. Onck, and E. van der Giessen, J. Mech. Phys. Solids **56**, 2240 (2008).
[46] C. P. Broedersz and F. C. MacKintosh, Soft Matter **7**, 3186 (2011).
[47] See Supplemental Material at http://link.aps.org/supplemental/10.1103/PhysRevE.85.021801 for the stiffening movie.
[48] M. Sheinman, C. P. Broedersz, and F. C. MacKintosh (unpublished).
[49] S. Feng, M. F. Thorpe, and E. Garboczi, Phys. Rev. B **31**, 276 (1985).
[50] L. M. Schwartz, S. Feng, M. F. Thorpe, and P. N. Sen, Phys. Rev. B **32**, 4607 (1985).
[51] X. Mao and T. C. Lubensky, Phys. Rev. E **83**, 011111 (2011).
[52] S. Alexander, Phys. Rep. **296**, 65 (1998).
[53] M. Born and K. Huang, *Dynamical Theory of Crystal Lattices* (Oxford University Press, New York, 1954).
[54] B. A. DiDonna and T. C. Lubensky, Phys. Rev. E **72**, 066619 (2005).
[55] J. Liu, G. H. Koenderink, K. E. Kasza, F. C. MacKintosh, and D. A. Weitz, Phys. Rev. Lett. **98**, 198304 (2007).
[56] V. L. Ginzburg, Sov. Phys. Solid State **2**, 1824 (1960).
[57] D. Ben-Avraham and S. Havlin, *Diffusion and Reactions in Fractals and Disordered Systems* (Cambridge University Press, Cambridge, UK, 2000).
[58] M. Sahimi, *Heterogeneous Materials* (Springer, New York, 2003).
[59] S. Kirkpatrick, Rev. Mod. Phys. **45**, 574 (1973).
[60] V. K. S. Shante and S. Kirkpatrick, Adv. Phys. **20**, 325 (1971).
[61] C. D. Lorenz and R. M. Ziff, Phys. Rev. E **57**, 230 (1998).
[62] M. Das, F. C. MacKintosh, and A. J. Levine, Phys. Rev. Lett. **99**, 038101 (2007).
[63] D. J. Jacobs and M. F. Thorpe, Phys. Rev. Lett. **80**, 5451 (1998).
[64] M. F. Thorpe, D. J. Jacobs, N. V. Chubynsky, and A. J. Rader, in *Rigidity Theory and Applications* (Kluwer, New York, 1999), p. 239.
[65] W. G. Ellenbroek, Z. Zeravcic, W. van Saarloos, and M. van Hecke, Europhys. Lett. **87**, 34004 (2009).
[66] X. Mao and T. C. Lubensky (unpublished).